MEASUREMENT OF THE RADIATIVE LIFETIMES OF THE $v = 1$ AND $v = 2$ LEVELS OF THE A STATE OF CARBON MONOXIDE

BY

RALPH LAURENCE BURNHAM

A DISSERTATION PRESENTED TO THE GRADUATE COUNCIL OF THE UNIVERSITY OF FLORIDA IN PARTIAL FULFILLMENT OF THE REQUIREMENTS FOR THE DEGREE OF DOCTOR OF PHILOSOPHY

UNIVERSITY OF FLORIDA
1972

ACKNOWLEDGMENTS

The author wishes to thank the members of his supervisory committee for their assistance throughout his graduate program. In particular he wishes to thank the chairman of his supervisory committee, Dr. Ralph C. Isler, for his guidance during the course of this research.

The author also wishes to thank Dr. William Wells for his assistance during the early stages of this research.

TABLE OF CONTENTS

	Page
ACKNOWLEDGMENTS	ii
LIST OF TABLES	v
LIST OF FIGURES	vi
ABSTRACT	vii
CHAPTER	
I. INTRODUCTION	1
II. THEORETICAL CONSIDERATIONS	7
Semiclassical Analog to the Level-Crossing Phenomenon	7
Quantum Mechanical Calculation of the Hanlé Effect Signal for the A State of CO	12
Rotational Line Contributions to the Molecular Level-Crossing Signal	20
Rotational Intensity Distribution in a Molecular Discharge	20
Rotational Intensities in Resonance Fluorescence	25
The Effect of Rotational Perturbations on the Level-Crossing Signal	30
Lifetimes, Transition Probabilities, f-Values, and r-Centroids of Molecular Transitions	33
III. EXPERIMENTAL APPARATUS	40
Molecular Discharge Lamp Design	43
Optical System	49
Detection Apparatus	53
Magnetic Field Control Circuitry	57

TABLE OF CONTENTS (Continued)

CHAPTER		Page
IV.	EXPERIMENTAL PROCEDURE	61
	Lamp Spectra	62
	Spectra of Scattered Light	66
	Analysis of the Hanlé Effect Signals	71
V.	RESULTS	78
	$v' = 1$	78
	Results for Unperturbed Levels	81
	Results for Perturbed Levels	82
	$v' = 2$	83
VI.	CONCLUSIONS	87
LIST OF REFERENCES		93

LIST OF TABLES

Table		Page
I.	Results of the Quantum Mechanical Calculation of the Hanlé Effect Signal for the A State of CO	22
II.	Contributions to the Hanlé Effect Signal from Excited Rotational States	73
III.	Experimental Results for Perturbed Rotational Levels .	85
IV.	Lifetimes of Vibrational Levels of the A State of CO .	89

LIST OF FIGURES

Figure		Page
I.	Semiclassical Analog to the Level-Crossing Phenomenon	9
II.	a. Coordinate System for the Molecular Level-Crossing Experiment b. Partial Energy Level Diagram for a $^1\Pi$-$^1\Sigma^+$ Molecular Transition	15
III.	Coordinate System for the Scattering Region	29
IV.	Experimental Apparatus	42
V.	Molecular Discharge Lamp	48
VI.	Scattering Cell	52
VII.	Control Circuitry for the Electromagnet	59
VIII.	Lamp Spectrum of the (1,0) Band	64
IX.	Fluorescent Spectrum of the (1,0) Band	68
X.	Fluorescent Spectrum of the (2,0) Band	70
XI.	Experimental Hanlé Effect Signal with Fitted Lineshape	77
XII.	Experimental Results for the $v = 1$ and $v = 2$ Vibrational Levels	80

Abstract of Dissertation Presented to the
Graduate Council of the University of Florida in Partial Fulfillment
of the Requirements for the Degree of Doctor of Philosophy

MEASUREMENT OF THE RADIATIVE LIFETIMES OF THE v = 1 AND v = 2 LEVELS OF THE A STATE OF CARBON MONOXIDE

By

Ralph Laurence Burnham

March, 1972

Chairman: Dr. Ralph C. Isler
Major Department: Physics

The technique of zero-field level-crossing spectroscopy was employed to obtain the radiative lifetimes of the v = 1 and v = 2 vibrational levels of the $A^1\Pi$ state of carbon monoxide. Level-crossing signals were obtained for eight individually resolved rotational features in the (1,0) vibrational band and for four individually resolved rotational features in the (2,0) vibrational band. The signals were found to consist of level-crossing lineshapes from only three rotational transitions, and were analyzed to yield values of $g_J\tau_J$, the product of the Landé g factor and the lifetime. Narrowing of the lineshapes of several of the rotational levels was observed in the v = 1 state. This effect was attributable to a perturbation caused by the $a'^3\Sigma^+$ state. The values of the coupling constants for the perturbed rotational levels were obtained from analysis of the level-crossing data. The experimental lifetimes of the v = 2 level and of the unperturbed states of the v = 1 level were obtained by calculating

the Landé g factor for the $^1\Pi$ state from Hund's case (a) coupling scheme. The lifetimes of individual rotational states within a level were averaged to yield the lifetime of the level. For the v = 1 level the result was $\tau_{v=1} = 10.41 \pm 0.8$ nsec. For the v = 2 level the result was $\tau_{v=2} = 8.49 \pm 1.0$ nsec.

CHAPTER I

INTRODUCTION

The bands of the fourth positive system of carbon monoxide which arise from transitions between vibrational levels of the $A^1\Pi$ state and the $X^1\Sigma^+$ state of the molecule have historically been of fundamental research interest. Original spectroscopic work was stimulated by the presence of intense fourth positive bands as a contaminant in spectra taken in the ultraviolet and vacuum-ultraviolet regions of the spectrum. Early workers investigated the structure of bands seen in both emission and absorption, and by 1940 vibrational and rotational analysis of all known bands was essentially complete [1].

Recent research has been devoted to the investigation of the lifetime, oscillator strengths, and perturbations of the $A^1\Pi$ state. Simmons et al. [2] have made accurate assignments of perturbations due to six known states in the region of the $A^1\Pi$ state. Their work was based on the analysis by Herzberg and others [3,4,5] of bands arising from forbidden transitions to the ground state. It is the upper states of these transitions which interact with the $A^1\Pi$ state giving rise to the observed perturbations.

Discovery of carbon monoxide bands in both the infrared and ultraviolet regions of the solar spectrum [6], as well as the prediction of the existence of the gas in interstellar space [7] has

emphasized the astrophysical importance of the molecule. Quite recently Mariners VI and VII have detected radiation from carbon monoxide bands produced in the upper layers of the Martian atmosphere [8,9]. Surprisingly, the observed Cameron bands which arise from a forbidden $^3\Pi - {}^1\Sigma^+$ transition were more intense than those of the fourth positive system. James [10] has derived expressions for the oscillator strengths of the Cameron bands by assuming a coupling between the $a^3\Pi$ and the $A^1\Pi$ states. An accurate knowledge of the fundamental properties of the $A^1\Pi$ state is thus becoming important for several aspects of astrophysical research.

Considerable controversy has developed over attempts to relate measured values of the lifetimes to oscillator strengths of the bands of the A-X transition. Hesser [11] obtained the lifetimes of several vibrational levels using the phase shift technique. These values were then used in conjunction with his measurement of the relative intensities of the bands to obtain a value of .094 for the absorption oscillator strength of the transition. The result was in conspicuous disagreement with the value, $f = .24$, obtained by Meyer et al. [12] from electron scattering data. In order to determine the source of the discrepancy, Wells and Isler [13] measured the lifetime of the $A(v' = 2)$ state using level-crossing spectroscopy. Their result was in substantial agreement with that of Hesser. The controversy was partially resolved by Mumma et al. [14] who remeasured the relative intensities of the vibrational bands using a system which had a calibrated spectral response. These measurements were normalized to the average of the

lifetime measurements and yielded a value of .15 for the integrated oscillator strength. Lawrence [15] also reanalyzed Hesser's data and obtained an f value of .17. These results may be compared to the value, f = .195 ± .012, obtained by Lassettre and Skerbele [16] through the comparison of elastically and inelastically scattered electrons. Meyer's measurements have also been refined [17] and the results are now consistent with those of Lassettre and Skerbele. The agreement between the values of the oscillator strength calculated from lifetime measurements and those obtained from electron impact experiments is thus considerably improved, but not perfect.

Mumma's intensity measurements also revealed a strong dependence of the electronic transition moment on the internuclear separation in the carbon monoxide molecule. This dependence produces a variation of the transition moment over the bands of the fourth positive system, and must be considered when calculating f values from radiative lifetimes. Mumma assumed a linear relation between the transition moment and the r-centroid of the vibrational transition, and analysis of his intensity data gave

$$R_e \propto (1 - .60\bar{r}_{v'v''}) \qquad (1)$$

where R_e is the transition moment and $\bar{r}_{v'v''}$ is the r-centroid of the $(v'v'')$ vibrational band. This relation was in good agreement with the data of Lassettre and Skerbele. Some doubt has been cast upon the relationship of equation 1 by the recent lifetime measurements of Imhof and Read [18]. Their data, obtained for $v' = 0$ through $v' = 6$ levels

by the delayed coincidence technique, indicate a quadratic or higher dependence of the transition moment on the r-centroid. Chervenak and Anderson [19] have also calculated a quadratic dependence from lifetime information obtained from an experiment employing a pulsed invertron. The validity of their data is, however, open to question.

The work described in this dissertation was undertaken in order to obtain accurate radiative lifetimes of individual vibrational levels of the $A^1\Pi$ state of carbon monoxide. The experimental results contained herein will most certainly prove useful in determining the oscillator strengths and transition moments of bands of the fourth positive system.

The level-crossing phenomenon which was employed to obtain the lifetime measurements reported in this work was first discovered by Hanlé [20] in 1924. Level-crossing signals are produced when two or more magnetic sublevels of an excited atomic or molecular state become degenerate at a particular magnetic field. The degenerate sublevels are excited coherently. Re-emitted radiation from the sublevels suffers interference, giving rise to an alteration in the polarization and angular distribution of the observed light. When the signal arises from the degeneracy in the Zeeman levels at zero magnetic field, the level-crossing phenomenon is known as the Hanlé effect. The phenomenon was explained by Breit [21] in 1933, but lay unexploited until accidentally rediscovered by Colgrove et al. [22] in 1959. Since then, level-crossing spectroscopy has proved to be an excellent technique for measuring a variety of fundamental properties of excited states of atomic systems.

Quite recently level-crossing spectroscopy has begun to be applied to the measurement of properties of diatomic molecules. The technique is quite similar to that used with atoms but in general experimental procedure is complicated by the vibrational and rotational structure of the molecular electronic states. The effects of level crossings in diatomic molecules were derived from Breit's original formula by Zare [23] who also suggested several systems as possible subjects for investigation. The first molecular level-crossing signals were reported for NO by Crosley and Zare [24]. Unfortunately their results were later found to be spurious and due to mercury contamination of their experiment [25]. Several molecular systems have now been successfully treated. Silvers et al. [26] have observed signals from individual rotational levels of CS excited by overlapping atomic lines from Mn II. DeZafra et al. [25] have used molecular resonance radiation to excite individual rotational levels in the OH and OD radicals, and have combined level-crossing and optical double resonance data to determine lifetimes and g factors for excited states of these species. In a slightly different approach, Wells and Isler [13] used radiation from an entire vibrational band to excite the $v' = 2$ level of the $A^1\Pi$ state of carbon monoxide. Contributions to the level-crossing signal from each rotational line present in the scattered radiation were then assessed in the analysis of their data.

In the experiment described in this dissertation resonance radiation produced in a molecular discharge lamp was used to excite high rotational levels in the $v' = 1$ and $v' = 2$ vibrational levels of

the $A^1\Pi$ state of carbon monoxide. The level-crossing signals obtained were shown to consist of contributions from only three unresolved rotational lines, and proved to be amenable to analysis by curve-fitting techniques. The basic experimental quantity obtained from the data analysis was the product of the lifetime and the Landé g factor for the vibrational-rotational state under investigation. A theoretical value for the g factor was obtained by assuming a case (a) coupling scheme for the $A^1\Pi$ state. The experimental value of the radiative lifetime was thus obtained. Narrowing of the observed lineshapes was quite evident for several of the levels in the $v' = 1$ state. This distortion of the Hanlé effect signals was attributed to a rotational perturbation in the $A^1\Pi$ state. Data from the perturbed levels were analyzed to obtain values for the parameters characteristic of the perturbation.

CHAPTER II

THEORETICAL CONSIDERATIONS

In this section the theoretical lineshapes for Hanlé effect signals arising from $A^1\Pi - X^1\Sigma^+$ transitions in carbon monoxide will be developed. In addition, since the exciting radiation employed in this experiment consisted of a superposition of three unresolved rotational lines, a mathematical model will be constructed which will allow the contribution to the level-crossing signal from transitions from each excited rotational level within a vibrational state to be assessed. Finally, the effects of a rotational perturbation in the $A^1\Pi$ upper state upon the level-crossing line shape will be developed using basic perturbation theory.

Semiclassical Analog to the Level-Crossing Phenomenon

Some of the basic features of the zero-field level-crossing phenomenon (Hanlé effect) may be easily understood if one considers the following semiclassical analog to the exact quantum system.

An electronic transition in an atom or molecule may be represented classically as an electric dipole with components p_x, p_y, and p_z. The upper state of the transition has a magnetic moment, $\vec{\mu}_o$, as shown in figure I. In an ideal experimental arrangement exciting

Figure I: Semiclassical Analog to the Level-Crossing Phenomenon

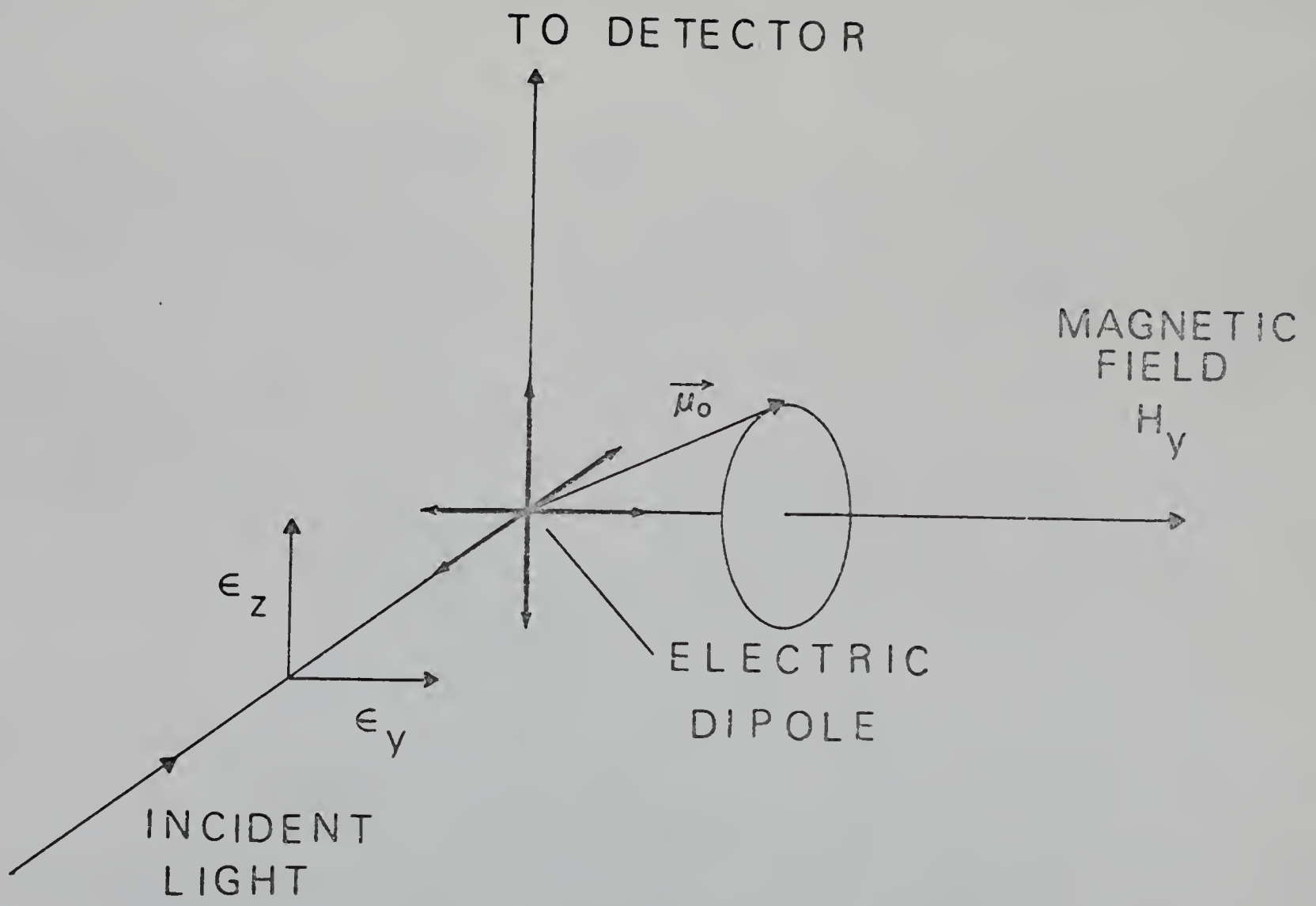
TO DETECTOR
MAGNETIC FIELD
H_y
$\vec{\mu_o}$
ϵ_z
ϵ_y
ELECTRIC DIPOLE
INCIDENT LIGHT

radiation with polarization vectors, $\vec{\epsilon}_y$ and $\vec{\epsilon}_z$, is incident along the x axis. Light scattered by the atom is detected along the z axis. A magnetic field, $\vec{H}$, may be applied along the y axis.

If initially the magnetic field is zero, only light associated with the y component of the electric dipole will reach the detector. If now a magnetic field is applied as shown in figure I, the magnetic moment will precess about the y axis with the Larmor frequency,

$$\omega_L = \left(\frac{g_J \mu_o}{\hbar}\right) \vec{H} . \tag{2}$$

The radiated intensity observed along the z axis will then be given by

$$\bar{I}_t = c \int_o^\infty e^{-t/\tau} \sin^2 \omega_L t \, dt . \tag{3}$$

Integration yields

$$\bar{I}_t = \frac{c'}{2} \left[1 - \frac{1}{1+(2g_J \mu_o \tau H/\hbar)^2} \right] . \tag{4}$$

In the above integral $\sin^2 \omega_L t$ gives the intensity of radiation associated with the precessing dipole, and the damping term, $e^{-t/\tau}$, is included to account for the decay of the dipole associated with the emission of radiation. In addition to the field-dependent level-crossing signal, a constant background due to radiation from the y component of the electric dipole will also be observed unless the polarization of the incident radiation is chosen to exclude excitation of this component.

The level-crossing signal has the form of an inverted Lorentizian lineshape having $\bar{I}_t = 0$ at $\vec{H} = 0$. If $H_{\frac{1}{2}}$ is the magnetic field necessary to produce $\frac{1}{2}$ maximum intensity, then τ, the lifetime of the state is given by

$$g_J \tau = \frac{\hbar}{2\mu_o H_{\frac{1}{2}}} . \tag{5}$$

Thus if the g factor of the radiating state is known, the lifetime is given by a simple measurement of the halfwidth of the experimentally obtained Lorentzian lineshape.

The semiclassical analog is also useful for understanding the effects on the level-crossing signal of departures from the ideal experimental geometry given in figure I. Suppose that scattered light is detected in the x-z plane at an angle, θ, to the z axis. Then the $\sin^2 \omega_L t$ term in equation 3 must be replaced by $\sin^2(\omega_L t + \theta)$. Making this substitution, the intensity of light scattered into the detector will be given by

$$\bar{I}_t = c \int_o^\infty e^{-t/\tau} \sin^2(\omega_L t + \theta) dt$$

$$= \frac{c}{2} \int_o^\infty e^{-t/\tau} \left[1 - (\cos 2\omega_L t \cos 2\theta + \sin 2\omega_L t \sin 2\theta) \right] dt . \tag{6}$$

Integration of equation 6 yields

$$\bar{I}_t = \frac{c'}{2} \left[1 - \cos 2\theta \frac{R^2}{1+R^2} - \sin 2\theta \frac{R}{1+R^2} \right] \tag{7}$$

where

$$R = \frac{2\mu_o g_J H \tau}{\hbar} . \tag{8}$$

The level-crossing signal given by equation 7 now contains terms of both even and odd functional dependence on the magnetic field. The dependence on the detector angle, θ, must be taken into account under actual experimental conditions when the finite volume of the scattering region and the solid angle of the detector are considered.

Quantum Mechanical Calculation of the Hanlé Effect Signal for the A State of CO

The rate at which radiation is absorbed, exciting an individual molecular rotational level, and subsequently re-emitted into a single rotational branch is given by the Breit [21] formula,

$$\bar{I}(J,J',J'') \propto \sum_{\substack{\mu\mu' \\ mm'}} \frac{\langle J'\mu|\vec{f}\cdot\vec{r}|Jm\rangle\langle Jm|\vec{f}\cdot\vec{r}|J'\mu'\rangle\langle J'\mu'|\vec{g}\cdot\vec{r}|J''m''\rangle\langle J''m''|\vec{g}\cdot\vec{r}|J'\mu\rangle}{[1+i(\mu-\mu')\mu_o g_{J'}\tau_{J'}H/\hbar]} . \tag{9}$$

The vectors, $\vec{f}$ and $\vec{g}$, are the polarizations of the exciting and re-emitted radiation, respectively. J and J'', m and m'' are the quantum numbers related to the total angular momenta of the ground states and their projections on the space-fixed z axis, and J', μ and μ' are the corresponding quantum numbers for the excited state. In the denominator, $g_{J'}$ and $\tau_{J'}$ denote the Landé g factor and the lifetime of the excited state, and H is the magnetic field strength. The level-crossing signal is calculated by inserting the proper wavefunctions for the $^1\Pi$ excited state and the $^1\Sigma^+$ ground state into equation 9 and summing over all possible combinations of magnetic quantum numbers.

The wavefunction for the ground state may be expressed as the product of electronic and rotational functions

$$\psi(\Sigma^+)_J = \chi'_\eta(r',\theta')(2\pi)^{-1}[2(2J+1)]^{\frac{1}{2}} \mathcal{D}^{(J)}_{m',o}(\alpha\beta\gamma) \quad . \tag{10}$$

The coordinates, r' and θ', are defined with respect to a coordinate system in which z' corresponds to the internuclear axis of the molecule. The quantities α, β, and γ, are the Euler angles associated with the transformation which takes the space-fixed axes into the molecule-fixed coordinate system. (See figure IIa.) The elements of the rotation matrix, $\mathcal{D}$'s, may be shown to be the rotational eigenfunctions for the symmetric top molecule when multiplied by the normalizing factor, $[2(2J+1)]^{\frac{1}{2}}$ [27]. The wave functions for the Λ doubled $^1\Pi$ upper state are constructed in a similar fashion:

$$\psi(\Pi^\zeta)_{J'} = \chi_K(r'\theta')(4\pi)^{-1}[2(2J'+1)]^{\frac{1}{2}}\left[e^{i\Lambda\varphi'} \pm e^{-i\Lambda\varphi'}\right]$$

$$\cdot \left[\mathcal{D}^{(J')}_{\mu,\Lambda}(\alpha\beta\gamma) + \mathcal{D}^{(J')}_{\mu,-\Lambda}(\alpha\beta\gamma)\right] , \tag{11}$$

where ζ denotes either the c or d component of the doublet. The electronic parts of the wavefunctions for the upper state are either symmetric or antisymmetric under reflection in a plane which contains the internuclear axis of the molecule. This may be seen by making the substitution $\varphi' \rightarrow -\varphi'$ in equation 11. The $^1\Sigma^+$ state is symmetric under this reflection.

Figure II: a. Coordinate System for the Molecular Level-Crossing Experiment b. Partial Energy Level Diagram for a $^1\Pi$-$^1\Sigma^+$ Molecular Transition

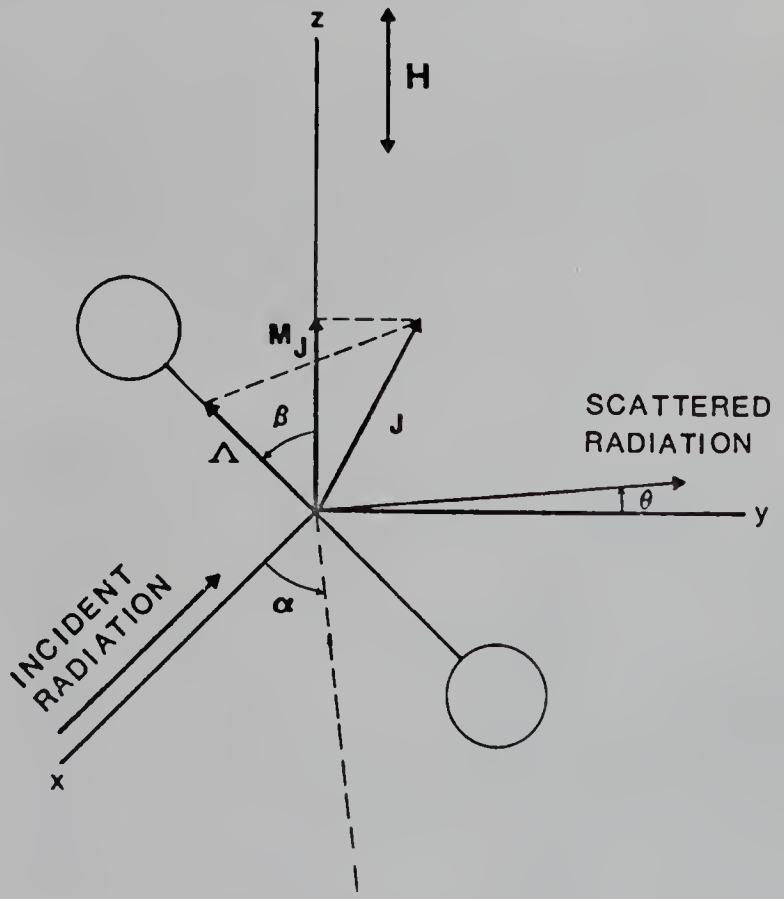
z
H
M_J
β
Λ
J
SCATTERED
RADIATION
θ
y
INCIDENT
RADIATION
α
x

(a)

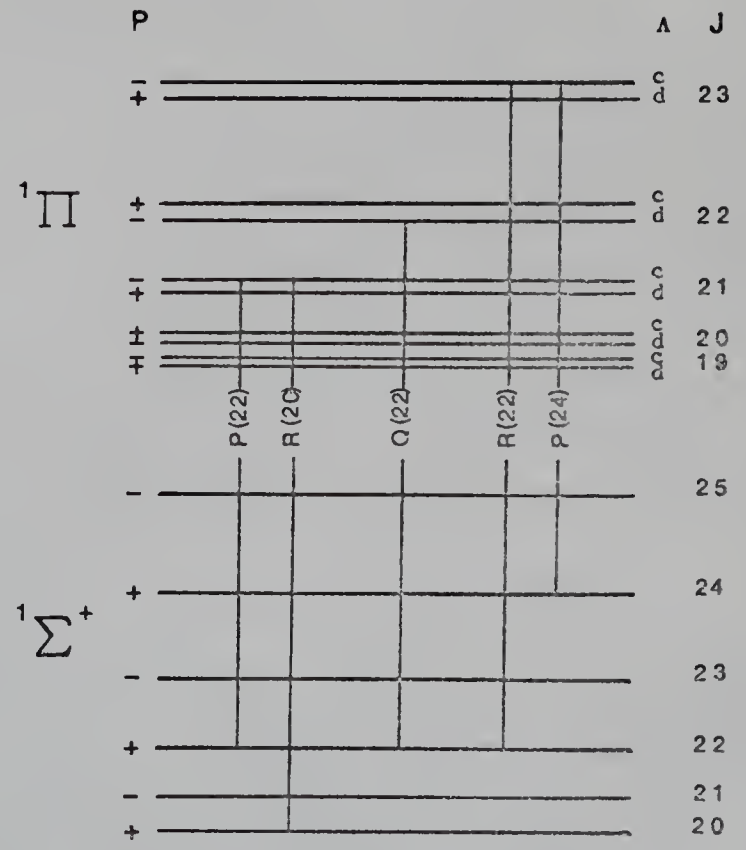
P
Λ
J
$^1\Pi$
$^1\Sigma^+$
P(22)
R(20)
Q(22)
R(22)
P(24)

(b)

The wavefunctions in equations 10 and 11 may also be seen to possess definite symmetry (parity) under an inversion, R, of the space-fixed coordinates through the origin. Under such a transformation

$$\alpha \rightarrow \pi + \alpha, \qquad \beta \rightarrow \pi - \beta, \qquad \gamma \rightarrow -\gamma,$$

and

$$\mathcal{D}^{(J)}_{m,\Lambda}(\pi+\alpha,\ \pi-\beta,\ -\gamma) = (-1)^{J-2m}\,\mathcal{D}^{(J)}_{m,-\Lambda}(\alpha,\beta,\gamma)\ . \tag{12}$$

Application of the transformation, R, to the wavefunctions yields the following results:

$$R\Psi(\Sigma^{+})_J = (-1)^J \Psi(\Sigma^{+})_J \tag{13a}$$

$$R\Psi(^1\Pi^c_d)_J = \pm(-1)^J \Psi(^1\Pi^c_d)_J\ . \tag{13b}$$

Thus the parity alternates as a function of even and odd values of J.

The operators such as $\vec{f}\cdot\vec{r}$ which appear in the Breit formula (equation 9) may be expanded as the scalar product of two spherical tensors with the components of $r^{(1)}$ expressed in terms of the rotating coordinate system

$$\vec{f}\cdot\vec{r} = \sum_{\lambda} (-1)^{\lambda} f^{(1)}_{-\lambda} r^{(1)}_{+\lambda} = \sum_{\lambda\nu} (-1)^{\lambda} f^{(1)}_{-\lambda}\,\mathcal{D}^{(1)}_{\lambda,\nu}(\alpha\beta\gamma)\, r^{(1)\prime}_{\nu}\ . \tag{14}$$

The dipole matrix elements appearing in the Breit formula are most readily evaluated by employing the relationship

$$\int_0^{2\pi}\int_0^{\pi}\int_0^{2\pi} \mathcal{D}^{(J_1)}_{m_1 m_1'}(\alpha\beta\gamma)\,\mathcal{D}^{(J_2)}_{m_2 m_2'}(\alpha\beta\gamma)\,\mathcal{D}^{(J_3)}_{m_3 m_3'}(\alpha\beta\gamma)\,d\alpha \sin\beta d\beta d\gamma$$

$$= (8\pi)^2 \begin{pmatrix} J_1 & J_2 & J_3 \\ m_1 & m_2 & m_3 \end{pmatrix}\begin{pmatrix} J_1 & J_2 & J_3 \\ m_1' & m_2' & m_3' \end{pmatrix}, \tag{15}$$

where the terms appearing on the right side of the equation are Wigner 3-j symbols. Integration over the molecule-fixed coordinates is facilitated by the use of orthogonality relationship,

$$\int_0^{\infty}\int_0^{\pi}\int_0^{2\pi} \chi_K^*(r'\theta')\,\chi_\eta'(r'\theta')e^{\pm i\Lambda\varphi'}\, r_\nu^{(1)'}\, dr' \sin\theta' d\theta' d\varphi'$$

$$= R_{K\eta}\,\delta_{\nu,\mp\Lambda}, \tag{16}$$

where the integration over φ' has been carried out, and the integration over r' and θ' is contained in $R_{K\eta}$.

Using equations 10 and 11 the matrix elements may be written as

$$\langle J'\mu|\vec{f}\cdot\vec{r}|Jm\rangle\,\langle Jm|\vec{f}\cdot\vec{r}|J'\mu'\rangle$$

$$= \sum_{\substack{\lambda\nu\\ \alpha\beta}} \langle J'\mu|(-1)^{\lambda} f^{(1)}_{-\lambda}\mathcal{D}^{(1)}_{\lambda\nu} r_\nu^{(1)'}|Jm\rangle\langle Jm|(-1)^{\alpha} f^{(1)}_{-\alpha}\mathcal{D}^{(1)}_{\alpha\beta} r_\beta^{(1)'}|J'm'\rangle$$

$$= \sum_{\substack{\lambda\nu\\ \alpha\beta}} \left(\frac{1}{4\pi^2}\right)^2 (2J+1)(2J'+1)(-1)^{\lambda+\alpha} f^{(1)}_{-\lambda} f^{(1)}_{-\alpha} \tag{17}$$

$$\cdot\left\{\left[\langle K\Lambda|r_\nu^{(1)'}|\eta 0\rangle \pm \langle K-\Lambda|r_\nu^{(1)'}|\eta 0\rangle\right]\left[\int\int\int\left(\mathcal{D}^{(J)*}_{\mu\Lambda} + \mathcal{D}^{(J)*}_{\mu,-\Lambda}\right)\cdot\mathcal{D}^{(1)}_{\lambda\nu}\mathcal{D}^{(J)}_{m0}\,d\tau\right]\right.$$

$$\cdot\left\{\left[\langle\eta 0|r_\beta^{(1)'}|K\Lambda\rangle \pm \langle\eta 0|r_\beta^{(1)'}|K-\Lambda\rangle\right]\left[\int\int\int\mathcal{D}^{(J)*}_{m0}\mathcal{D}^{(1)*}_{\alpha\beta}\cdot\left(\mathcal{D}^{(J)}_{\mu'\Lambda} + \mathcal{D}^{(J)}_{\mu',-\Lambda}\right)d\tau\right]\right.$$

Employing equations 15 and 16 and the property that

$$\mathcal{D}^{(J)*}_{\alpha,\beta} = (-1)^{\alpha+\beta}\,\mathcal{D}^{(J)}_{\alpha,-\beta}$$

equation 17 becomes

$$\langle J'\mu|\vec{f}\cdot\vec{r}|Jm\rangle\,\langle Jm|\vec{f}\cdot\vec{r}|J'\mu'\rangle$$

$$= \sum_{\substack{\lambda\nu\\ \alpha\beta}} \left(\frac{1}{4\pi^2}\right)^2 (2J+1)(2J'+1)(-1)^{\lambda+\alpha+\mu+m-\Lambda} \begin{matrix} f^{(1)} & f^{(1)} \\ -\lambda & -\alpha \end{matrix} |R_{K\eta}|^2 (8\pi)^4$$

$$\cdot \left[\begin{pmatrix} J' & 1 & J \\ -\mu & \lambda & m \end{pmatrix} \begin{pmatrix} J' & 1 & J \\ \Lambda & \nu & 0 \end{pmatrix} \pm \begin{pmatrix} J' & 1 & J \\ -\mu & \lambda & m \end{pmatrix} \begin{pmatrix} J' & 1 & J \\ -\Lambda & \nu & 0 \end{pmatrix} \right]$$

$$\cdot \left[\begin{pmatrix} J & 1 & J' \\ -m & \alpha & \mu' \end{pmatrix} \begin{pmatrix} J & 1 & J' \\ 0 & \beta & \Lambda \end{pmatrix} \pm \begin{pmatrix} J & 1 & J' \\ -\Lambda & \beta & 0 \end{pmatrix} \begin{pmatrix} J & 1 & J' \\ -m & \alpha & \mu' \end{pmatrix} \right] . \qquad (18)$$

The symmetry properties of the 3-j symbols may be used to write the matrix elements in their final form

$$\langle J'\mu|\vec{f}\cdot\vec{r}|Jm\rangle\,\langle Jm|\vec{f}\cdot\vec{r}|J'\mu'\rangle = \sum_{\lambda\alpha} 16(2J+1)(2J'+1)(-1)^{\lambda+\alpha+\mu+m+1}$$

$$\cdot \begin{matrix} f^{(1)}_{-\lambda} & f^{(1)}_{-\alpha} \end{matrix} |R_{K\eta}|^2 (-1)^{J+J'+1} \begin{pmatrix} J & J' & 1 \\ m & -\mu & \lambda \end{pmatrix} \begin{pmatrix} J & J' & 1 \\ m & -\mu' & \alpha \end{pmatrix}$$

$$\cdot \left[(1 \pm (1)^{J+J'+1}) \begin{pmatrix} J & J' & 1 \\ 0 & 1 & -1 \end{pmatrix} \right]^2 . \qquad (19)$$

The matrix elements for emission may be obtained in a similar manner. The final form of the Breit formula then becomes

$$\bar{I}(J,J',J'') \propto \sum_{\substack{mm''\mu\mu' \\ \lambda\sigma\delta\epsilon}} 16\left|R_{K\eta}\right|^4 (-1)^{2J'+J+J''+\mu+\mu'+m+m''+\lambda+\sigma+\delta+\epsilon}$$

$$\cdot\ (2J+1)(2J''+1)(2J'+1)^2\ f^{(1)}_{-\lambda}\ f^{(1)}_{-\sigma}\ g^{(1)}_{-\delta}\ g^{(1)}_{-\epsilon}$$

$$\cdot\ \left[1 \pm (-1)^{J+J'+1}\right]^2 \begin{pmatrix} J & J' & 1 \\ 0 & 1 & -1 \end{pmatrix}^2 \left[1 \pm (-1)^{J'+J''+1}\right]^2 \begin{pmatrix} J'' & J' & 1 \\ 0 & 1 & -1 \end{pmatrix}^2$$

$$\cdot\ \begin{pmatrix} J & J' & 1 \\ m & -\mu & \lambda \end{pmatrix} \begin{pmatrix} J & J' & 1 \\ m & -\mu' & -\sigma \end{pmatrix} \begin{pmatrix} J'' & J' & 1 \\ m'' & -\mu' & \delta \end{pmatrix} \begin{pmatrix} J'' & J' & 1 \\ m'' & -\mu & -\epsilon \end{pmatrix}$$

$$\cdot\ \left[1 + i(\mu-\mu')\mu_o g_{J'} \tau_{J'} H/\hbar\right]^{-1} . \qquad (20)$$

The terms $\left[1 + (-1)^{J'+J''+1}\right]$ and $\left[1 + (-1)^{J'+J+1}\right]$ in equation 20 arise from the selection rule which requires a parity change in absorption and emission of radiation. The terms indicate that excitation from a lower level, J, to an upper level, J', takesplace to a c state if $J' = J \pm 1$ and to a d state if $J' = J$, and that re-emission takes place in a similar fashion. A consequence of the parity selection rule is the prohibition of excitation through a Q branch followed by re-emission in a P or R branch and vice versa, as may be seen by examining the partial energy level diagram for $^1\Pi - {}^1\Sigma^+$ transitions (figure IIb).

The summation indicated in equation 20 is performed by first grouping terms for which $|\mu - \mu'| = 0,1$, or 2 and then summing over all possible sets of the indices λ, σ, δ, ϵ. The process is facilitated through the use of the sums,

$$\sum_{m=J}^{m=J} m^n = \begin{cases} 0 & n = \text{odd} \\ (2J+1) & n = 0 \\ (2J+1)J(J+1)/3 & n = 2 \\ (2J+1)J(J+1)(3J^2+3J-1)/15 & n = 4 \end{cases},$$

or, in certain cases, through the use of the defining relationship between 3-j and 6-j symbols.

Table I gives the result of the calculation for the $^1\Pi - {}^1\Sigma^+$ transition in carbon monoxide. Under the experimental conditions of unpolarized exciting and scattered radiation, terms for which $|\mu-\mu'| = 1$ cancel and the signal consists of a field-independent background which arises from terms for which $|\mu-\mu'| = 0$ and a field-dependent part which arises from terms for which $|\mu-\mu'| = 2$.

Rotational Line Contributions to the Molecular Level-Crossing Signal

In the following paragraphs a mathematical model will be developed which will allow the contributions of unresolved rotational lines to the level-crossing signal to be calculated. The calculation will be carried out by first determining the contributions of individual rotational lines to the intensity of a molecular discharge and then deriving the rate of resonance fluorescence from a scattering gas.

Rotational Intensity Distribution in a Molecular Discharge

The relative intensities of isolated rotational lines produced under conditions of thermal equilibrium may be expressed as the product

Table I: Results of the Quantum Mechanical Calculation of the Hanlé Effect Signal for the A State of CO

Table I

$\overline{I}_{J,J';J''}$

Absorption - J" \ Emission - J"	J'-1 (R)	J'(Q)	J'+1 (P)
J'-1 (R)	$\frac{(J'+1)^2}{J'(2J'-1)(2J'+1)}$ $((54J'^2-25J'+1)+A(J'+1)(2J'+3))$	———	$\frac{J'(J'+1)}{2J'+1}$ $(27+A)$
J'(Q)	———	$((28J'^2+28J'-1)+A(2J'+3)(2J'-1))$	———
J'+1 (P)	$\frac{J'(J'+1)}{2J'+1}$ $(27+A)$	———	$\frac{J'^2}{(2J'+3)(2J'+1)(J'+1)}$ $((54J'^2+133J'+120)+AJ'(2J'-1))$

$A = (\cos 2\varphi + R \sin 2\varphi)/(1+R^2)$, $R = 2g_{J'}\tau_{J'}\mu_o H/\hbar$

$\varphi = 90^o + \theta$

of the line strength of the transition and the temperature dependent Boltzmannfactor divided by the rotational partition function

$$I(J',J'') = \frac{i(J',J'')\exp\,[-B'J'(J'+1)hc/kT_L]}{Q_{rot}} \quad . \tag{21}$$

Here B' is the rotational constant for the upper state, T_L is the effective rotational temperature for the discharge, and the rotational partition function is given by kT_L/hcB' for all but very low temperatures. The line strength is given by the Hönl-London factor for the transition. For a $^1\Pi - {}^1\Sigma^+$ transition in a symmetric top molecule these factors are

$$\begin{aligned} i(J',J') &= (2J'+1)/2 \\ i(J',J'-1) &= (J'+1)/2 \\ i(J',J'+1) &= J'/2 \end{aligned} \tag{22}$$

for the Q, R, and P branches, respectively.

The relative intensity and shape of a Doppler broadened rotational line produced in a layer of gas of thickness dx in a discharge lamp of uniform cross section is given by

$$d\mathcal{A}(\nu,J',J'') = I(J',J'')k_o \exp\left[-\frac{2\nu}{\Delta\nu_D}\sqrt{\ell n\, 2}\right]^2 dx \quad . \tag{23}$$

The parameter, k_o, is the absorption coefficient of the gas and the Doppler breadth of the line, $\Delta\nu_D$, may be written as

$$\Delta\nu_D = \frac{2\sqrt{2k\,\ell n\, 2}}{c}\,\nu_o\sqrt{\frac{T}{m}} \quad . \tag{24}$$

The distance in wavenumber from the center of the line is given by ν. The contribution to the output intensity at the front of the lamp ($x = 0$) from the element dx is

$$ds(\nu,J',J'') = I(J',J'')k_o \exp\left[-\frac{2\nu}{\Delta\nu_D}\sqrt{\ell n\, 2}\right]^2$$

$$\cdot \exp\left[-k_o I_\ell(J',J'')x \exp\left(-\frac{2\nu}{\Delta\nu_D}\sqrt{\ell n\, 2}\right)^2\right] dx \ , \qquad (25)$$

where the second term accounts for absorption present in the lamp. It is assumed here that once a photon has been absorbed it is lost to the output of the lamp. The relative absorption from molecules in the lower state is given by

$$I_\ell(J',J'') = \frac{i(J',J'') \exp\left[-B''J''(J''+1)hc/kT_L\right]}{Q_{rot}} \qquad (26)$$

where B'' is the rotational constant of the lower state. Integration over the length of the lamp gives the contribution to the intensity from a frequency band $d\nu$:

$$s(\nu,J',J'')d\nu = LI(J',J'')\left[\alpha_L I_\ell(J',J'')\right]^{-1}$$

$$\cdot \left\{1 - \exp\left[-\alpha_L I_\ell(J',J'') \exp\left(-\frac{2\nu}{\Delta\nu_D}\sqrt{\ell n\, 2}\right)^2\right]\right\} d\nu \ . \qquad (27)$$

The effective absorption coefficient for the discharge has been defined as $\alpha_L = k_o L$. The total intensity from an isolated rotational line is found by integrating over the Doppler profile of the line

$$S(J',J'') = \int_0^\infty s(\nu,J',J'')d\nu \quad . \tag{28}$$

The simulated spectrum for an entire molecular band is generated by forming a sum of the rotational line intensities over the wavelength region of the band:

$$\mathscr{I}(\lambda) = \sum_{\lambda_i=\lambda_{min}}^{\lambda_{max}} T(\lambda-\lambda_i)S(\lambda_i(J',J'')) \quad . \tag{29}$$

The parameters, λ_{min} and λ_{max}, give the lower and upper wavelength limits of the band, λ_i is the wavelength of a particular rotational line characterized by the upper and lower quantum numbers (J',J''), and $T(\lambda-\lambda_i)$ is the triangular bandpass function of the monochromator used to resolve the spectrum. The bandpass function is defined as

$$T(\lambda) = \begin{cases} \left|1 - \left|\lambda/\Delta\lambda\right|\right| & \left|\lambda/\Delta\lambda\right| \leq 1 \\ 0 & \left|\lambda/\Delta\lambda\right| \end{cases} \tag{30}$$

where $\Delta\lambda$ is the resolution of the monochromator and is assumed to be much larger than the width of the rotational lines.

Rotational Intensities in Resonance Fluorescence

Calculation of the intensity of radiation absorbed and re-emitted by the scattering gas proceeds in a fashion similar to the calculation of the lamp intensity. For a particular mode of absorption followed by re-emission characterized by the rotational

quantum numbers, $J'' \rightarrow J' \rightarrow J$, the intensity of light scattered into a detector at approximately right angles to the incident beam is given by

$$I(\alpha_s,J,J',J'') \propto \int_0^D dz \int_0^{4\pi} d\Omega \int_0^{\infty} S(J',J'')A(\alpha_s,J',J'')\bar{I}(J,J',J'')d\nu \ . \tag{31}$$

$S(\nu,J',J'')$ is the incident radiation intensity. The intensity of radiation absorbed and re-emitted by the scattering gas is given by the product, $A(\alpha_s,J',J'')\bar{I}(J,J',J'')$, where

$$A(\alpha_s,J',J'')dz = \alpha_s M(T_s,J'') \exp\left(-\frac{2\nu}{\Delta\nu_D}\sqrt{\ell n\, 2}\right)^2$$

$$\cdot \exp\left[-\alpha_s I_\ell(T_s,J,J')z \exp\left(-\frac{2\nu}{\Delta\nu_D}\sqrt{\ell n\, 2}\right)^2\right] dz \ . \tag{32}$$

The parameters, α_s and T_s, are the absorption coefficient and temperature of the scattering gas, and

$$M(T_s,J'') = \frac{\exp\left[-B''J''(J''+1)hc/kT\right]}{Q_{rot}} \tag{33}$$

gives the relative populations of the ground state rotational levels. The rate at which radiation is absorbed and re-emitted by the scattering gas is given by $\bar{I}(J,J',J'')$. This is the term which was calculated above from the molecular Breit formula, and contains the dependence on the magnetic field and scattering angle.

Integration over z, the length of the scattering region, and Ω, the solid angle subtended by the detector at the point of scattering,

accounts for departures from the ideal right angle scattering geometry. The geometry of the scattering region is shown in figure III. If y represents the distance along the detector face, the differential area element on the detector face may be written as

$$dA(y) = 2(2ay-y^2)^{\frac{1}{2}}\, dy \ . \tag{34}$$

The solid angle subtended by dA(y) is then

$$d\Omega = (2ay-y^2)^{\frac{1}{2}} \left[(z-y)^2 + a^2\right]^{\frac{3}{2}} dy, \tag{35}$$

where "a" gives the distance from the center of the exciting beam to the detector. Equation 35 holds only approximately if the detector is not sufficiently removed from the scattering region. However, the error introduced by this approximation is small compared to other uncertainties present in this analysis. In addition, it has been assumed that the exciting radiation is confined to a narrow beam along the central axis of the scattering region. While this is not strictly the case under actual experimental conditions, it may be seen that scattering angles from above and below the center line tend to average to the scattering angle, θ.

The integral in equation 31 is readily evaluated with a digital computer, using the Conroy [28] routine for multiple integrals.

Figure III: Coordinate System for the Scattering Region

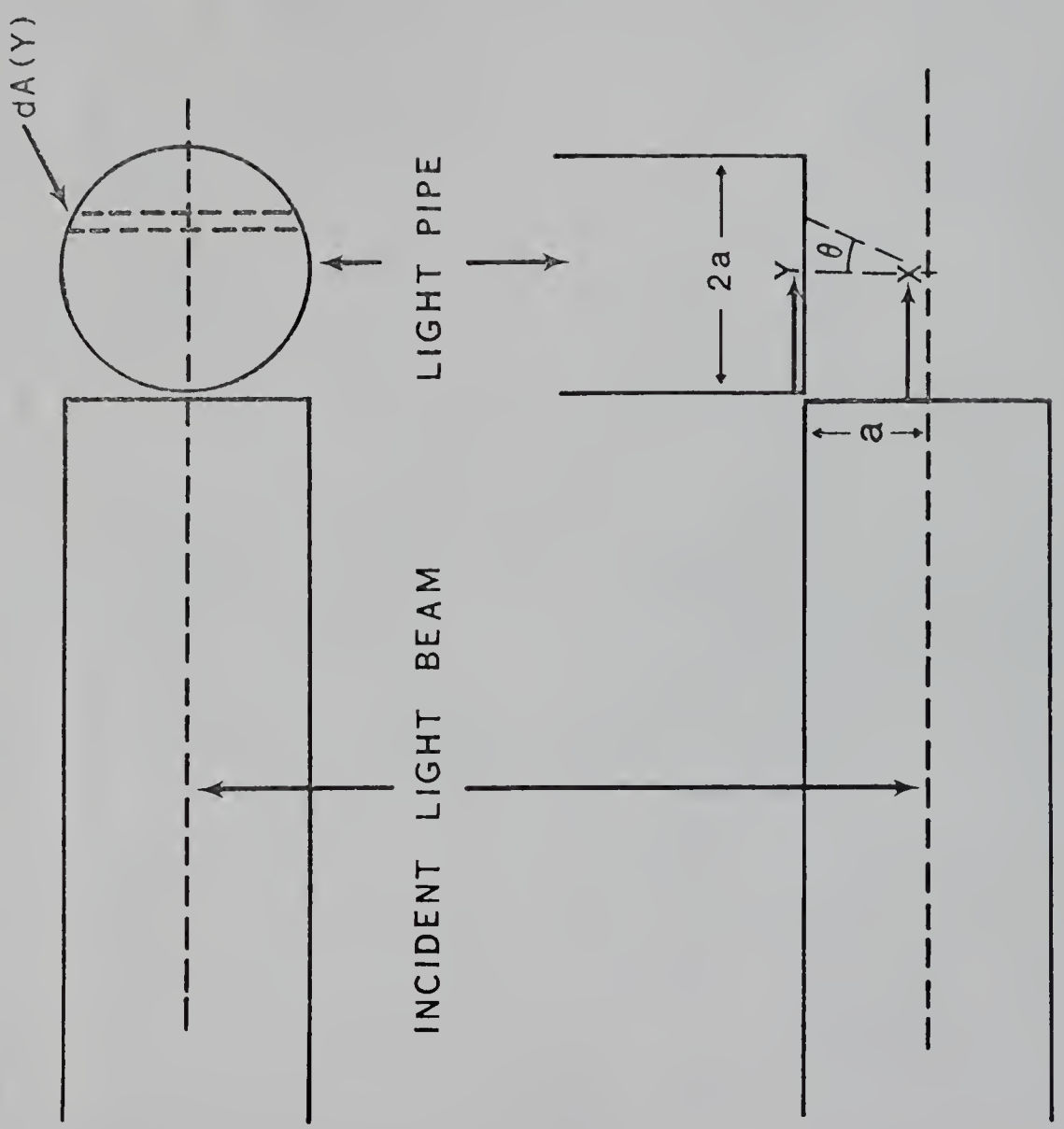
dA (Y)
LIGHT PIPE
INCIDENT LIGHT BEAM
2a
Y
θ
a

The Effect of Rotational Perturbations on the Molecular Level-Crossing Signal

The $A^1\Pi$ state of carbon monoxide is characterized by the many perturbations which result from the mixing of the $A^1\Pi$ state with another state of the molecule. The coupling of two states of nearly equal energy arises from terms omitted from the Hamiltonian and produces shifts from the expected rotational energy progressions within a vibrational level. In addition, if the coupling is sufficiently strong, additional lines will appear in the spectrum of the vibrational band. To see the effect of a perturbation of a rotational level upon the level-crossing signal let the wavefunction of the $A^1\Pi$ state be represented by $|A,J\rangle$ and that of the perturbing state by $|B,J\rangle$. A selection rule (see Herzberg [29, p. 285]) prohibits the mixing of states of different rotational quantum number. It will be assumed that m_J remains a good quantum number for the range of the magnetic field encountered in the level-crossing experiment. This assumption is justified for the types of terms being considered in the perturbation calculation.

A perturbation which couples two molecular states, $|A,J\rangle$ and $|B,J\rangle$, gives rise to the two mixed states with wavefunctions,

$$\Psi_1 = \alpha|A,J\rangle - \beta|B,J\rangle \ , \tag{36}$$

and

$$\Psi_2 = \beta|A,J\rangle + \alpha|B,J\rangle \ , \tag{37}$$

where

$$\alpha^2 + \beta^2 = 1 \ . \tag{38}$$

If the unperturbed energies of the states are designated by E_A and E_B, then the perturbed energies will be given by

$$E_{\pm} = \frac{(E_A+E_B) \pm \sqrt{(E_A-E_B)^2 + 4\Delta^2}}{2} , \tag{39}$$

where Δ is the matrix element of the perturbation term, P, between the two states:

$$\Delta = \langle A,J|P|B,J\rangle . \tag{40}$$

The coupling coefficients, α and β, may be written as

$$\alpha = \left(\frac{\sqrt{(E_A-E_B)^2 + 4\Delta^2} + (E_A-E_B)}{2\sqrt{(E_A-E_B)^2 + 4\Delta^2}} \right)^{\frac{1}{2}} \tag{41}$$

and

$$\beta = \left(\frac{\sqrt{(E_A-E_B)^2 + 4\Delta^2} - (E_A-E_B)}{2\sqrt{(E_A-E_B)^2 + 4\Delta^2}} \right)^{\frac{1}{2}} . \tag{42}$$

Using equations 39, 41 and 42, it can be shown that Δ may be written as

$$\Delta^2 = \frac{\alpha^2(E_A-E_B)^2(1-\alpha^2)}{(2\alpha^2 - 1)^2} . \tag{43}$$

The Zeeman energy for the mixed state, Ψ_1 may be obtained through the following considerations. The Zeeman energy is written as

$$E_z = \left[(\alpha^* \langle A| - \beta^* \langle B|) \vec{\mu} \cdot \vec{H} (\alpha |A\rangle - \beta |B\rangle) \right] , \tag{44}$$

or

$$E_z = |\alpha|^2 \langle A| \vec{\mu} \cdot \vec{H} |A\rangle + |\beta|^2 \langle B| \vec{\mu} \cdot \vec{H} |B\rangle . \tag{45}$$

Thus

$$\begin{aligned} E_z &= |\alpha|^2 \mu_o g_J(A) H m_J + |\beta|^2 \mu_o g_J(B) H m_J \\ &= \mu_o H \left[|\alpha|^2 g_J(A) + |\beta|^2 g_J(B) \right] m_J , \end{aligned} \tag{46}$$

where $g_J(A)$ and $g_J(B)$ are the molecular g factors for the states A and B, respectively. The Zeeman energy may now be written as

$$E_z = \mu_o \bar{g}_J H m_J , \tag{47}$$

if the effective g factor for the mixed state is defined as

$$\bar{g}_J = [\alpha^2 g_J(A) + \beta^2 g_J(B)] . \tag{48}$$

From equation 5, the relationship between the product, $g_J \tau_J$, for the perturbed state and the experimental halfwidth of the level-crossing signal becomes

$$\bar{g}_J \tau_J = \frac{\hbar}{2 \mu_o H_{\frac{1}{2}}} . \tag{49}$$

If the lifetime of state B is long compared to that of state A, the lifetime of the perturbed level will be given by

$$\tau_J = \tau_A / \alpha^2 , \tag{50}$$

where τ_A is the lifetime of the pure A state. Then using equations 48 and 50, equation 49 may be written as

$$\bar{g}_J \tau_J = \left(\alpha^2 g_J(A) + \beta^2 g_J(B)\right) \frac{\tau_A}{\alpha^2} = \frac{\hbar}{2\mu_o H_{\frac{1}{2}}} \tag{51}$$

or

$$g_J(A) + \frac{(1-\alpha^2)}{\alpha^2} g_J(B) = \frac{\hbar}{2\mu_o \tau_A H_{\frac{1}{2}}} \quad . \tag{52}$$

Thus, if the g factors and approximate lifetimes for the two states participating in the perturbation are known, the coupling constants may be obtained from the experimental level-crossing data. If, in addition, the term values for the perturbing states are known from spectroscopic analysis, equation 43 may be employed to obtain Δ, the strength of the perturbation.

Lifetimes, Transition Probabilities, f-Values, and r-Centroids of Molecular Transitions

The discrepancy between the results of certain experiments involving measurements of the fundamental properties of the $A^1\Pi$ state of carbon monoxide has been discussed in Chapter I. These discrepancies arose, in part, from attempts to relate absorption oscillator strengths calculated from measured radiative lifetimes to those obtained directly in electron impact experiments. In the following paragraphs a discussion is given of the theory which may be used to relate some of the fundamental quantities obtained in experiments involving

electronic transitions in simple molecules. The discussion is based on the treatment of molecular quantum mechanics outlined by Herzberg [29], and the discussion of transition probabilities given by James [10].

The Schrödinger equation of a diatomic molecule may be written as

$$\frac{1}{m}\sum_i \nabla_i^2\psi + \sum_k \frac{1}{M_k}\nabla_k^2\psi + \frac{8\pi^2}{h^2}(E-V)\psi = 0 \ , \tag{53}$$

where i refers to the coordinates of the electrons (mass m) and k refers to those of the nuclei (mass M_k). An approximate solution to equation 53 may be written as $\psi = \psi_e(\vec{r}_i)\psi_{vr}(\vec{r}_k)$ where ψ_e and ψ_{vr} are solutions of the equations

$$\sum_i \nabla_i^2\psi_e + \frac{8\pi^2 m}{h^2}(E^{el}-V_e)\psi_e = 0 \tag{54}$$

and

$$\sum_k \frac{1}{M_k}\nabla_k^2\psi_{vr} + \frac{8\pi^2}{h^2}(E-E^{el}-V_n)\psi_{vr} = 0, \tag{55}$$

respectively. The first of these equations is the Schrödinger equation for electrons moving in the field of fixed nuclei and having a potential energy, V_e. For different internuclear distances V_e is different and therefore the eigenfunctions, ψ_e, and the eigenvalues, E^{el}, of this equation depend on the internuclear distance as a parameter. The second equation is the Schrödinger equation of the nuclei moving under the action of the potential energy, $E^{el} + V_n$, where V_n is the Coulomb

potential energy of the nuclei. It may be shown that the expression given above for the total eigenfunction is a solution to equation 53 only if the variation of ψ_e with the internuclear distance may be neglected. This condition is fulfilled for most diatomic molecules and is known as the Born-Oppenheimer approximation. The use of $E^{el} + V_n$ as the potential energy for the motion of the nuclei and the resolution of ψ into the product of ψ_e and ψ_{vr} is therefore usually justified.

The intensity of an electronic transition from an upper state, a, to a lower state, b, is determined by the transition probability, A_{ab}. The transition probability is in turn determined by the square of the dipole matrix element between the upper and lower states. Under the assumption that the Born-Oppenheimer approximation holds, the matrix element may be written as

$$R = \langle \psi_{vr}^{a} | R(r) | \psi_{vr}^{b} \rangle \ . \tag{56}$$

The matrix element, R(r), is the electronic transition moment given by

$$R(r) \propto \langle \psi_{e}^{a} \mid \sum_{i} \vec{r}_i \mid \psi_{e}^{b} \rangle \ . \tag{57}$$

If the variation of R(r) with the internuclear distance is slow, R(r) may be replaced by its average for the vibrational transition. Equation 56 then becomes

$$R = \bar{R}_e \langle \psi_{vr}^{a} | \psi_{vr}^{b} \rangle \ . \tag{58}$$

Further, the vibrational-rotational overlap integral may be written as

$$\langle \psi^{a}_{vr} | \psi^{b}_{vr} \rangle = \langle v' | v'' \rangle R^{J'J''}_{rot} \quad , \tag{59}$$

where the first term is the square root of the Franck-Condon factor for the vibrational transition, and the second term is the overlap integral for the rotational transition.

The transition probability for emission, $A_{ab,v'v'',J',J''}$, is given by

$$A_{ab,v'v'',J'J''} = \frac{64\pi^4 \nu^3_{v'v''}}{3hd_a} \sum_{m'm''} |R|^2 \quad , \tag{60}$$

where the sum is over all values of the magnetic quantum numbers, m' and m''. The parameter, d_a, the degeneracy of the upper state, is equal to $2J' + 1$ for Σ states. States for which $\Lambda \geq 1$ are Λ doubled and therefore the degeneracy is $2(2J'+1)$. Summing over all possible rotational transitions from the upper state gives

$$A_{ab,v'v''} = \frac{64\pi^4 \nu^3_{v'v''}}{3h} |\bar{R}_e|^2 |\langle v' | v'' \rangle|^2 \tag{61}$$

on account of the sum rule,

$$\sum_{J'',mm''} |R^{J'J''}_{rot}|^2 = (2J'+1) \quad . \tag{62}$$

The transition probability is therefore independent of the rotational quantum number.

The transition probability for emission from a particular electronic-vibrational state may be written as

$$A_{v'} \equiv \sum_{v''} A_{v'v''} = \frac{64\pi^4}{3h} \sum_{v''} \nu^3_{v'v''} \left|\bar{R}_e(\bar{r}_{v'v''})\right|^2 \left|\langle v' | v'' \rangle\right|^2 . \qquad (63)$$

It should be noted that equation 63 applies to states for which only one route of decay to the lower state is allowed. For states which exhibit electronic branching, the sum in equation 63 must be taken over all states to which transitions occur. The electronic transition moment appearing in equation 63 has been written as a function of the average internuclear separation for the (v',v'') transition. The parameter, $\bar{r}_{v'v''}$, is known as the r-centroid of the transition, and gives a measure of the separation. The r-centroid is defined as

$$\bar{r}_{v'v''} = \frac{\langle v' | r | v'' \rangle}{\langle v' | v'' \rangle} . \qquad (64)$$

The lifetime of the electronic-vibrational state is given by

$$\tau_{v'} = \frac{1}{A_{v'}} . \qquad (65)$$

The transition moment, $\bar{R}_e$, may be taken to be constant for some molecules and removed from the sum in equation 63. In other cases the variation of ν over the vibrational band system may be neglected. Under these approximations, and in view of the sum rule, $\sum_{v''} \left|\langle v \, | v'' \rangle\right|^2 = 1$, the lifetime becomes

$$\frac{1}{\tau_{v'}} = \frac{64\pi^4 \nu^3}{3h} \bar{R}^2_e . \qquad (66)$$

In this approximation the lifetimes of all vibrational levels become equal. A more correct formula could be obtained by replacing ν^3 by the mean cubed wavenumber, $\langle\nu\rangle^3 = \sum_{v''}' \nu_{v''}^3 |\langle v'|v''\rangle|^2$. For the case where the variation of ν^3 with v'' can be neglected but $\bar{R}_e$ is not constant, equation 63 yields

$$A_{v'} = \frac{64\pi^4\nu^3}{3h} \langle v'|R_e^2(r)|v'\rangle \ , \tag{67}$$

where use has been made of the completeness relationship, $\sum_{v''}' |v''\rangle\langle v''| = 1$. Thus when ν^3 does not vary strongly with v'', lifetime measurements may be used to obtain information about the dependence $\bar{R}_e$ on the internuclear distance provided that Franck-Condon factors for the vibrational transitions are known.

The oscillator strength or f-value gives the degree to which a transition resembles a classical oscillating dipole in the absorption or re-emission of radiation. The f-value is given by

$$f_{v'v''} = \frac{1.499}{\nu_{v'v''}^2} \left(\frac{G'}{G''}\right) A_{v'v''} \ , \tag{68}$$

where the degeneracy factors, G's, are given by (2S+1) for Σ states and 2(2S+1) for states for which $\Lambda \geq 1$. The absorption oscillator strength or integrated f-value may be defined as

$$f_o = \sum_{v'}' f_{v'o} \ . \tag{69}$$

The absorption oscillator strength may, in principle, be related to the radiative lifetime through the use of equations 63, 65 and 68.

The bands of the fourth positive system of carbon monoxide extend over such a large wavelength region that the variation of ν may not be neglected. In addition, the strong dependence of the electronic transition moment on the internuclear distance has been well established. The assumptions which simplify the expression for the transition probability are therefore not appropriate to the bands of the A-X transition in carbon monoxide.

The f-values of the A-X transitions may be related to the lifetimes of the vibrational levels by employing equation 63 in conjunction with a model for the dependence of the electronic transition moment on the r-centroids of the vibrational transitions. It is usually assumed that $\bar{R}_e$ is a simple function of r-centroid. The parameters characteristic of the functional dependence are varied in equation 63 to obtain the best fit to the set of radiative lifetimes of the vibrational levels. Using the values of $\bar{R}_e$, the absorption oscillator strength may be calculated from equations 68 and 69. The use of this particular technique of analysis has produced the reasonable agreement between oscillator strengths calculated from lifetime values and those measured directly in electron scattering experiments.

CHAPTER III

EXPERIMENTAL APPARATUS

A diagram of the apparatus used for the molecular Hanlé effect experiment is shown in figure IV. Radiation for the excitation of the scattering gas was produced in a molecular discharge lamp. A one-meter vacuum monochromator was used to select bands of the fourth positive system of carbon monoxide. A beam of resonance radiation passed from the monochromator into the scattering cell where the proper geometry for the entrance beam, detector, and magnetic field was maintained. The scattering cell was mounted between the pole-pieces of an electromagnet capable of providing fields up to 10,000 Gauss. Resonance fluorescence from the scattering gas was shifted to a wavelength of about 4000 Å by a coating of sodium salycilate on the lower end of a lucite light pipe. The light was detected by a photomultiplier tube mounted in a field-free chamber. After amplification and time-constant smoothing, the signal, proportional to the photon counting rate for scattered resonance radiation, was stored in the memory of a signal averager as a function of the magnetic field in the scattering region. The stored signal could be obtained from a digital printer and from an X-Y plotter.

Figure IV: Experimental Apparatus

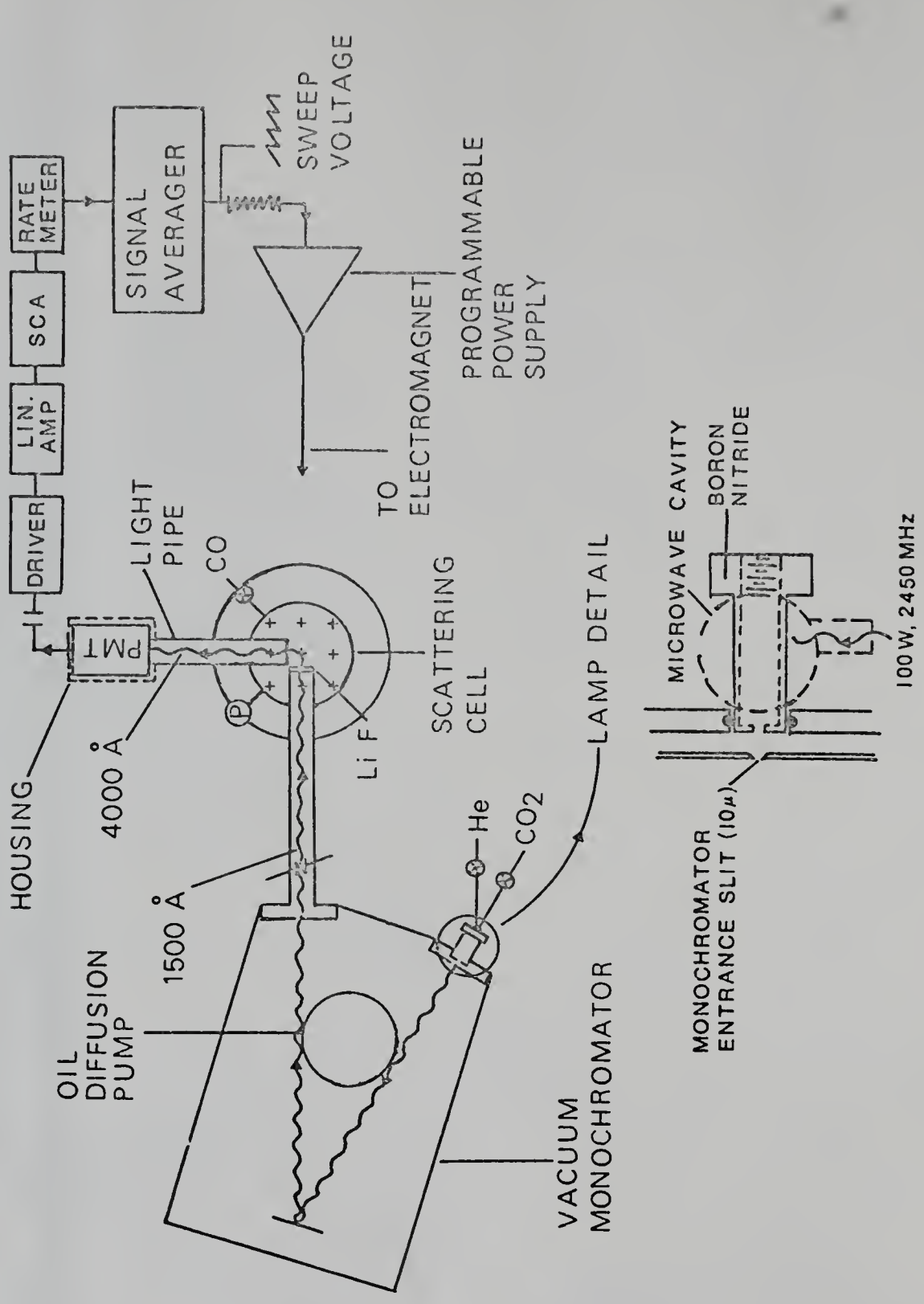
RATE METER
SCA
LIN. AMP
DRIVER
SIGNAL AVERAGER
SWEEP VOLTAGE
PROGRAMMABLE POWER SUPPLY
TO ELECTROMAGNET
LIGHT PIPE
CO
PMT
HOUSING
4000 Å
1500 Å
Li F
SCATTERING CELL
He
CO_2
LAMP DETAIL
OIL DIFFUSION PUMP
VACUUM MONOCHROMATOR
MICROWAVE CAVITY
BORON NITRIDE
MONOCHROMATOR ENTRANCE SLIT (10μ)
100 W, 2450 MHz

Molecular Discharge Lamp Design

In the molecular Hanlé effect experiment, one of the most difficult of experimental problems proved to be the development of a satisfactory source of radiation for the excitation of the scattering gas. The need for relatively large intensities in the bands of the fourth positive system suggested the use of a molecular discharge source. In addition to the need for high intensity, two other factors were present for consideration in the design of the discharge lamp. The first consideration was the reduction of self-reversal of the resonance radiation emitted by the lamp. Self-reversal occurs when a layer of unexcited gas lies between the emitting layer and the exit port of the lamp. Under this condition the line profile for the emitted radiation may exhibit a minimum at the center of the line. Self-reversed radiation is, of course, very ineffective in the excitation of the scattering gas. Fortunately, the absorption line strengths were relatively small for the high rotational levels investigated in this experiment, and most discharges were found to be optically thin, thus minimizing the problem of self-reversal.

The second and most important concern was the minimization of fluctuations in the intensity of the lamp. Since the level-crossing signal amounted to only a few percent of the total scattered light, nonstatistical fluctuations in intensity had to be kept low for the signal to be seen at all. It was found that the most stable radiation sources were those excited by radio frequency power.

The first type of lamp tried was a McPherson Model 630 ultraviolet light source as modified by Wells [30]. This source was basically a flow lamp in which the discharge took place in a mixture of helium and carbon dioxide in a water cooled capillary tube between aluminum electrodes. Helium flowed in a reverse direction through the lamp to help prevent self-reversal. The discharge was excited by a diathermy machine capable of producing up to 500 watts of R. F. power at 27 Mhz. Impedance matching between the lamp and the R. F. generator produced low standing wave ratios into the lamp under operating conditions. As an aid to reducing fluctuations in intensity, large ballast bottles were employed between the lamp and the gas supply tanks. The lamp was found to produce resonance radiation which was relatively free from self-reversal; however, the high R.F. power necessary for the operation of the lamp caused severe interference with the electronic apparatus used throughout the experiment. Serious attempts were made to shield against the spurious radiation before the use of the lamp was finally abandoned.

Extensive use of lamps excited by microwave energy in atomic level-crossing [31] and optical pumping [32] work suggested that a lamp of this type might prove equally useful in the molecular Hanlé effect experiment. In a microwave discharge the power is usually coupled into the gas through a resonant cavity, permitting the use of electrodeless lamps which are less susceptible to deterioration due to contamination. In addition, higher output intensities may be obtained with an expenditure of less excitation energy than with lower frequency

discharges due to the close coupling between the discharge and the power source. Bearing these factors in mind, several lamps were designed to be used with a Raytheon microwave power generator which produced up to 80 watts output at 2450 Mhz. These lamps were all constructed in such a way that the output radiation was emitted through a differential pumping port located at the front of the lamp. This design was chosen because LiF and MgF_2, the only materials suitable for windows in the wavelength region of interest (around 1500 Å), exhibit rapid deterioration in transmission upon exposure to intense ultraviolet radiation [33,34]. Several investigators [30,35,36] have reported useful lifetimes of only a few hours for discharge lamps with LiF windows. Differentially pumped lamps, on the other hand, were found to run indefinitely with no diminution of output intensity.

In the first source constructed, the discharge was carried in a 1/2-inch-diameter vicor ignition tube which was situated along the axis of a cylindrical $TM_{0,1,0}$ [37] cavity. Gasses were admitted at the back of the tube through a side arm. The lamp produced adequate intensity in the ultraviolet region but exhibited serious instability under certain operating conditions. This behavior was judged to be due to the limited number of modes available to the exciting radiation in the cavity. At certain pressures the lamp was seen to oscillate between two modes of excitation with an accompanying oscillation in intensity. In addition, the vicor tube was found to dissipate a sizable part of the microwave energy as heat. In order to overcome these difficulties, a second design was developed, utilizing a more

sophisticated Evans [38] type microwave cavity. This lamp is shown in detail in figure IV and in figure V. The Evans cavity was machined from brass stock and included both tuning and coupling adjustments. The lower portion of the cavity contained the discharge lamp itself which was machined from grade HP boron nitride. This material, a practically lossless dielectric in the microwave region, proved to be ideal for the confinement of the discharge. The discharge was carried within a 1/4-inch-diameter blind hole drilled along the axis of the boron nitride piece. Differential pumping took place across a 1/4-inch × 1 mm counter bore at the front of the lamp. This slit also served as an exit port for the vacuum ultraviolet radiation. Gas was admitted through a Swagelock fitting which was screwed into the central bore at the back of the lamp. The entire apparatus, lamp and cavity, was designed to be mounted on the slit housing of the monochromator as close to the entrance slits as possible. Differential pumping was accomplised by a large diffusion pump contained within the monochromator. The flow of gas into the back of the lamp, and consequently the gas pressure within the lamp, was regulated by two needle valves.

In operation, helium and carbon dioxide flowed into the back of the lamp, and the pressures of the two gasses were adjusted to produce the maximum output intensity in the molecular band of interest. Helium was found to produce a stable discharge in which the dissociation of the carbon dioxide and the excitation of the resulting carbon monoxide could take place. The use of carbon dioxide proved to be

Figure V: Molecular Discharge Lamp

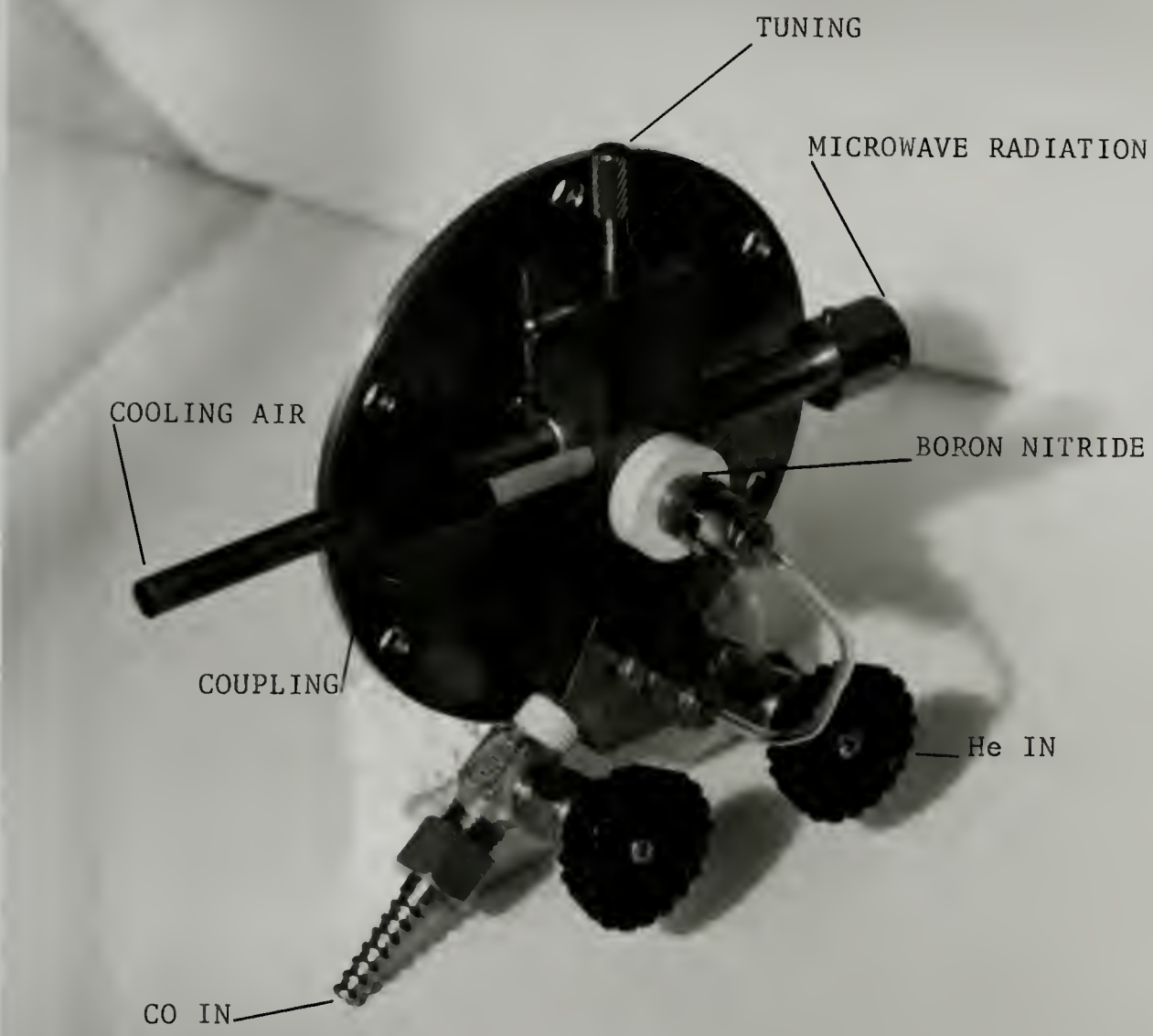
TUNING
MICROWAVE RADIATION
COOLING AIR
BORON NITRIDE
COUPLING
He IN
CO IN

helpful in preventing self-reversal of the molecular resonance radiation. The Evans microwave cavity allowed very low standing wave ratios to be obtained under almost all pressure conditions in the lamp. It was found that a pressure differential of about 10^4 could be maintained across the differential pumping slit, so that during operation the pressure in the monochromator was kept below 10^{-4} Torr. It was estimated from absorption in the spectrum of radiation emitted by the lamp that the partial pressure of carbon monoxide in the monochromator was not more than 10^{-7} Torr.

Optical System

For the purpose of description in this paper, that part of the experimental apparatus following the exit port of the discharge lamp and preceding the photomultiplier tube shall be designated as the optical system. Included in the optical system are the monochromator, the scattering cell, and the fluorescent detector and light pipe.

The bands of the fourth positive system of carbon monoxide were selected, using a McPherson Model 225 one-meter vacuum monochromator. This instrument was equipped with a large oil diffusion pump and could be evacuated to a pressure of less than 10^{-7} Torr. The monochromator was of normal incidence geometry and employed a cylindrical replica grating of one-meter radius to disperse the radiation. The grating measured 56 mm x 96 mm and was ruled with 600 lines per mm. With this grating the monochromator had a first-order reciprocal

dispersion of 16.6 Å/mm. With the entrance and exit slits set at 10 microns - a typical setting for the level-crossing experiment - the monochromator had a resolution of .166 Å. Light impinging upon the entrance slit was focused on the exit slit by the grating, and from there a diverging beam entered the scattering cell by the way of a hollow pipe of about one-half-meter length. The scattering cell was separated from the monochromator by a one-half-inch-diameter × 1-mm-thick LiF window.

The scattering cell was machined from aluminum in the form of an octagonal cylinder. A diagram of the scattering cell is given in figure VI. The cylinder was 2 inches thick, and the distance between the faces of the octagon was 6 inches. The scattering region was a two-inch-diameter × 5/8-inch-thick cylinder machined into the center of the scattering cell. Ports led from the scattering region to seven of the eight faces of the cell. Admission and removal of the scattering gas, as well as the entrance and exit of radiation, was through these ports. Gas was exhausted from the scattering region by a mechanical vacuum pump, and a base pressure of 5×10^{-4} Torr could be attained. Admission of carbon monoxide, the scattering gas, was through a micrometering valve. Under typical experimental conditions the pressure of the scattering gas was maintained at about 50 microns as measured by a Teledyne Model 2A thermocouple vacuum gauge.

A light pipe made of one-half-inch-diameter lucite rod extended into the scattering region to a position directly above, and adjacent to the entrance window. The lower tip of the light pipe was coated

Figure VI: Scattering Cell

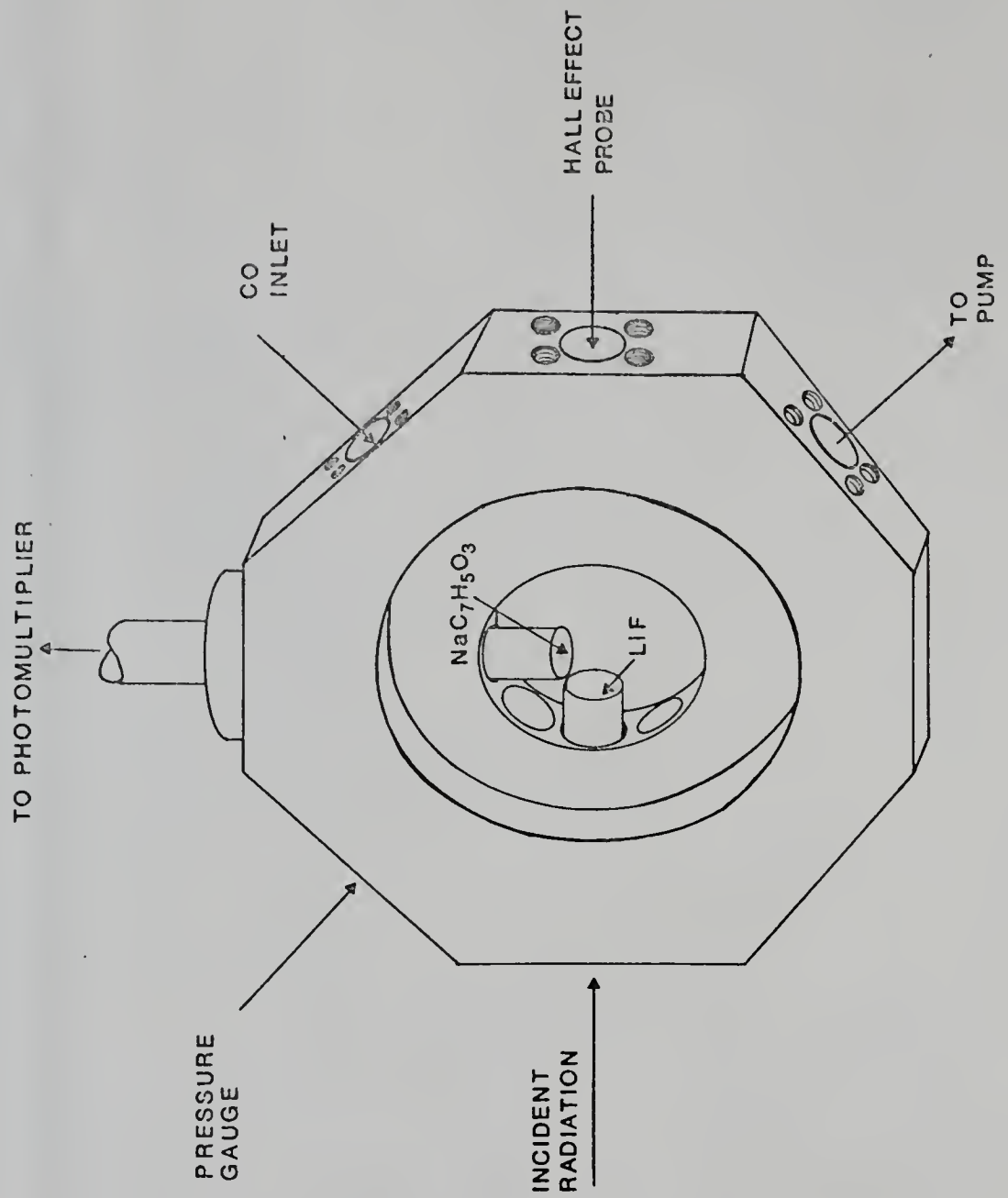
TO PHOTOMULTIPLIER
CO
INLET
HALL EFFECT
PROBE
TO
PUMP
$NaC_7H_5O_3$
LIF
PRESSURE
GAUGE
INCIDENT
RADIATION

with a thin deposit of sodium salycilate which fluoresced at about 4000 Å when struck by the scattered ultraviolet radiation. The fluorescent emission was propagated up the light pipe by internal reflection.

The scattering region was positioned between the 2-inch-diameter faces of the tapered pole pieces of the electromagnet. Spacing of the pole pieces was 3/4 inch.

Detection Apparatus

Light emitted by the sodium salycilate was detected by an EMI Model 6256S photomultiplier tube. The 1-cm-diameter photocathode of the tube was positioned directly above the polished upper tip of the light pipe. The response curve of the CsSb photocathode of the photomultiplier exhibited a maximum sensitivity at a wavelength which matched the output wavelength of the sodium salycilate. Overall efficiency of the detection system, scintillator, lightpipe, and photocathode, was judged to be somewhat less than 10 percent at an input wavelength of 1500 Å.

The photomultiplier along with its voltage-divider chain was mounted in a thermoelectrically cooled light-tight housing. Within the housing the photomultiplier tube was cooled to around 0°C. The dark counting rate for the tube at this temperature was between 10 sec^{-1} and 20 sec^{-1}. This rate was a factor of 50 below the counting rate for scattered light encountered in the level-crossing experiment. The housing also contained several concentric layers of "netic" and

"conetic" magnetic shielding material. In addition, the photomultiplier tube itself was surrounded by a mu-metal shield. Extensive magnetic shielding of the photomultiplier tube was necessary to assure that the sensitivity of the tube remained constant as the magnetic field was swept through its full range. With all of the shielding in place, the field at the location of the tube was found to vary by less than .2 Gauss as the field on the outside of and perpendicular to the cylinder axis of the housing was changed from 0 to 1000 Gauss. The sensitivity of the tube was found to change by less than .1 percent under these same circumstances. Systematic error introduced by the sensitivity of the photomultiplier tube to magnetic fields was negligible since the field-dependent component of the level-crossing signal always amounted to more than 2 percent of the intensity of the scattered light.

A potential of 1000 volts was maintained across the dynode chain of the photomultiplier tube. The voltage was supplied by stabilized high voltage power supply. The anode of the photomultiplier was maintained at ground potential. Output pulses from the tube were coupled to a wideband preamplifier through a 500 pfd capacitor. This capacitor in combination with the output load resistor of the photomultiplier tube formed a filter which yielded pulses with a width of about 5 μsec. The preamplifier was run at unity gain and served to drive several feet of 53 ohm coaxial cable. Output pulses from the preamplifier were transmitted along the coaxial cable to a linear amplifier. The gain of this amplifier could be varied from 60 to 400 and was set so that the largest input pulses just drove the amplifier to

full output. The pulses passed from the linear amplifier into a single channel analyzer. This device generated a pulse of precise shape each time it received a pulse whose height exceeded a certain threshold which could be set manually. In practice, the threshold was set to just exclude those noise pulses generated in the pre-amplifier.

In order to reduce noise fluctuations in the level-crossing signal, the output pulses from the single channel analyzer were fed into a ratemeter. In this instrument the series of input pulses was converted into a more slowly fluctuating analog voltage proportional to the counting rate. The conversion was accomplished by electronically integrating the input signal. The ratemeter contained a simple RC filter circuit which converted the input voltage, $V_i(t)$, into an output voltage given by

$$V_o(t) = k \int_{-\infty}^{t} e^{-(t-s)/RC} V_i(s) ds \qquad (70)$$

where RC was the time constant of the filter. The time constant was set so that only a small distortion was introduced into the shape of the level-crossing signal. The setting depended upon the rate at which the magnetic field was swept through its range, but time constants of a few tenths of a second were usually employed.

The output of the ratemeter was amplified to a level of a few volts and passed into the digitizer of the Fabri-Tek Model 1062 instrument computer which was used as a signal averager. In order to accomplish this amplification, the output of the ratemeter, which was only

10 millivolts, full scale, was boosted to a level of a few volts by a General Radio Type 1230-A electrometer. In the digitizer the analog signal was converted to digital form which allowed it to be stored in the memory of the instrument computer.

The use of the instrument computer as a signal averager proved to be essential to the detection of the level-crossing signal; under ordinary operating conditions the field-dependent part of the scattered light intensity was never found to exceed the statistical fluctuation in the total intensity. With counting rates of 1000 sec^{-1}, and an integrating time constant of .5 second, the field-dependent signal and the statistical fluctuation both amounted to about 3 percent. With signal averaging, the signal to noise ratio could be increased to a more useful level. This was possible, since, as counts were collected in the memory of the instrument computer, the field-dependent signal was accumulated in direct proportion to N, the number of counts; whereas the statistical noise increased as $\sqrt{N}$. Thus the signal to noise ratio was proportional to $\sqrt{N}$. The memory of the signal averager consisted of 1024 channels, each of which could retain up to 2^{18} counts. In practice, only one-fourth of the memory or 256 channels was utilized during an experimental run. The channels were addressed sequentially, and the number of counts stored in each was proportional to the voltage level appearing at the input of the digitizer at the time the channel was addressed. As the channels were addressed, the magnetic field in the scattering region was stepped through its range. Thus the level-crossing signal was stored as a function of the independent variable,

the magnetic field. The rate at which the field was swept depended on the dwell time for each channel utilized in the memory. Dwell times of .05 and .02 seconds per channel were most often used. The time constant of the counting system was adjusted to be equal to approximately 10 channels (i.e., .2 and .5 second, respectively, for the dwell times given above). For a dwell time of .05 second per channel, a sweep of the complete range of the field took place in .05 $\times$ 256 or 12.8 seconds. The signal stored in the memory was monitored on an oscilloscope and readout was accomplished with a Farbi-Tek digital printer. Data could also be plotted as a function of channel number on an X-Y plotter.

Magnetic Field Control Circuitry

The magnetic field in the scattering region was produced by an Alpha Model 4800 electromagnet. A diagram of the control and power circuitry for the electromagnet is given in figure VII. The basic control voltage for the experiment was supplied by the instrument computer. This voltage, which varied between 0 and 4 volts, was proportional to the number of the channel being addressed, and was used to drive two bipolar operational amplifiers. The amplifiers served as buffers for isolating the two legs of the circuit. Two Kepco Model JQE 36-30 power supplies were used to drive the electromagnet. These supplies could be voltage programmed and could supply up to 30 amperes at 40 volts. Programming voltagesfor the supplies

Figure VII: Control Circuitry for the Electromagnet

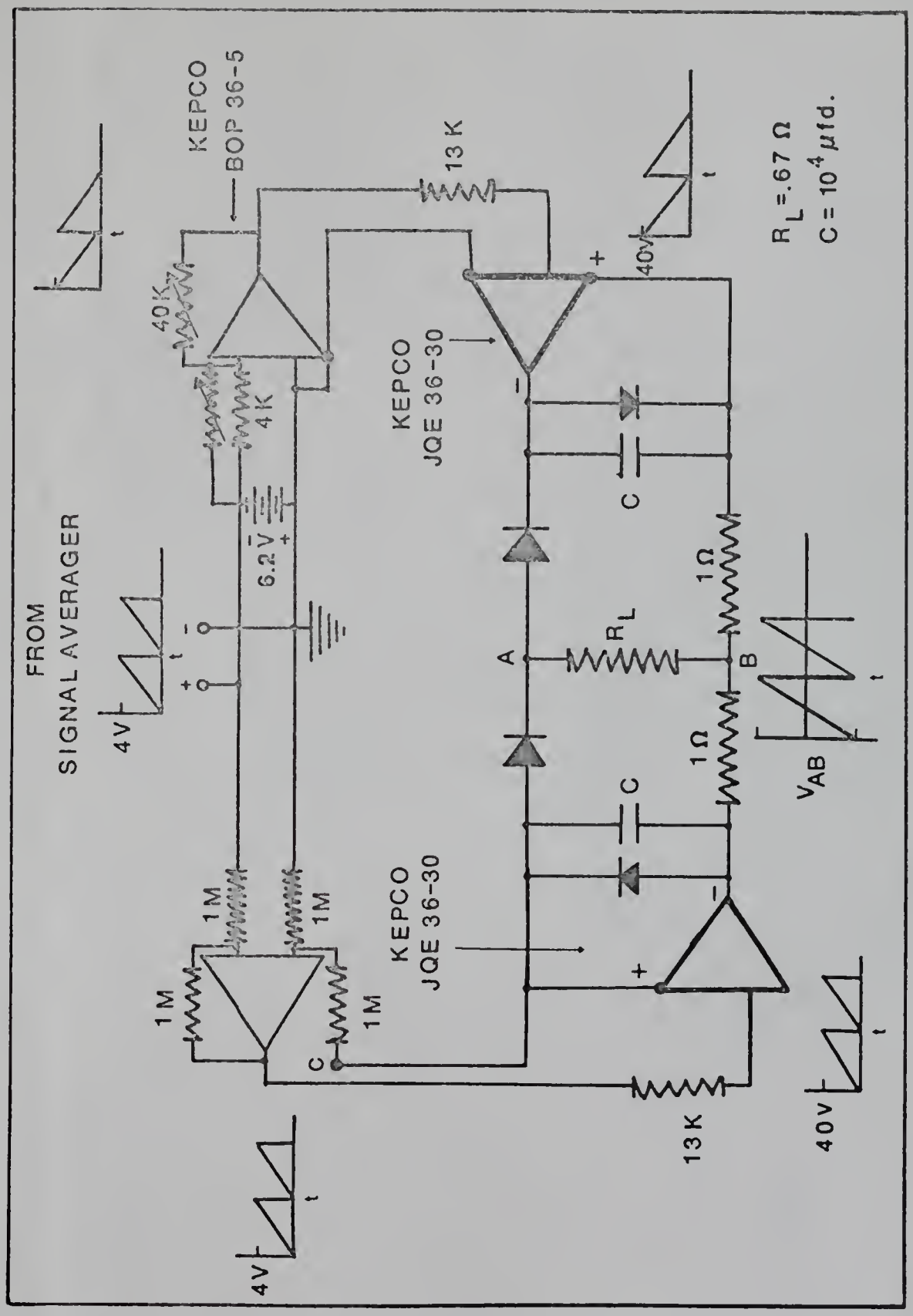
FROM
SIGNAL AVERAGER
4V
t
KEPCO
BOP 36-5
40K
4K
6.2V
1M
1M
1M
1M
C
KEPCO
JQE 36-30
13 K
40V
KEPCO
JQE 36-30
A
B
R_L
1Ω
1Ω
C
C
V_{AB}
13K
40V
R_L=.67 Ω
C= 10^{-4} μfd.

were taken from the output of the operational amplifiers. The waveforms of the programming voltages in figure VII show that as one supply was stepped from its minimum to its maximum output voltage, the other was stepped in the opposite direction. The voltage across the electromagnet therefore passed through zero at the middle of each sweep. Use of the circuit in figure VII resulted in the dissipation in the one-ohm resistors of over one-half of the power generated by the supplies, but the ability to sweep smoothly through zero field made the power waste tolerable. At the end of each sweep a transient was introduced as the energy stored in the magnetic field was fed back into the circuit. The capacitors and series and parallel diodes were placed in the circuit to help protect the power supplies from overvoltages and reverse polarities. A delay after each sweep allowed the circuit to come to equilibrium before a new sweep was started.

The field in the scattering region was monitored by a Hall effect probe. It was found that the field sweep was reproducible and had a maximum range of from 10,000 Gauss to -10,000 Gauss. The effects of hysteresis in the magnet were small. Corrections for nonlinearity in the field sweep were included in the analysis of the level-crossing signal. The Hall effect probe was calibrated periodically in a proton magnetic resonance spectrometer. The field within the scattering region was found to be homogeneous to within 1 percent.

CHAPTER IV

EXPERIMENTAL PROCEDURE

Molecular Hanlé effect experiments were initiated with the recording of the spectrum of the (1,0) band of the fourth positive system of carbon monoxide from the molecular discharge lamp. The spectrum was taken in order to determine the characteristic temperature and absorption coefficient of the discharge, and the (1,0) band was chosen because it is relatively free from overlapping bands of the fourth positive system. Although spectra were not taken before each experimental run, they were recorded periodically and the conditions in the lamp were found to be reproducible. A spectrum of the light scattered by the carbon monoxide gas sample was next recorded for the molecular band under investigation. From this spectrum the effective absorption coefficient of the scattering gas as well as the relative contributions to the Hanlé effect signal from excited rotational levels were determined. The Hanlé effect experiment itself was begun by centering the bandpass of the monochromator on a particular rotational feature of the band under investigation, and by adjusting the range of the magnetic field to be swept. Ordinarily the sweep was set to cover a range of about 14,000 Gauss centered on zero magnetic field. A plot of the magnetic field versus the channel number in the memory of the signal averager was taken in order to

determine the linearity and range of the sweep. The collection of level-crossing data in the memory then commenced and was continued until the quality of the experimental line shape reached the desired level. Generally, an experimental run lasted from two to four hours. At the end of the run the spectrum of scattered light was again recorded to assure that experimental conditions had not changed drastically. The level-crossing data were then fitted to theoretical line shapes with the aid of a digital computer.

Lamp Spectra

Ideally, molecular lifetime determinations using level-crossing spectroscopy would be performed on isolated rotational levels within a vibrational state. In experiments on the fourth positive system of carbon monoxide, this ideal could not be realized, since, for the bands investigated, the higher rotational lines tended to be arranged in closely spaced triplets. The components of these triplets could not be individually resolved by the monochromator. It was therefore necessary to assess the contribution to the level-crossing signal from each rotational state of the scattering molecules excited by a component of the unresolved triplet.

An example of a spectrum of the (1,0) band obtained from the discharge lamp is given in figure VIII. In obtaining the spectrum the detector was mounted directly on the exit slit housing of the monochromator. The discharge in the lamp was begun and allowed to stabilize. Helium pressure in the lamp was then adjusted until the partial pressure

Figure VIII: Lamp Spectrum of the (1,0) Band

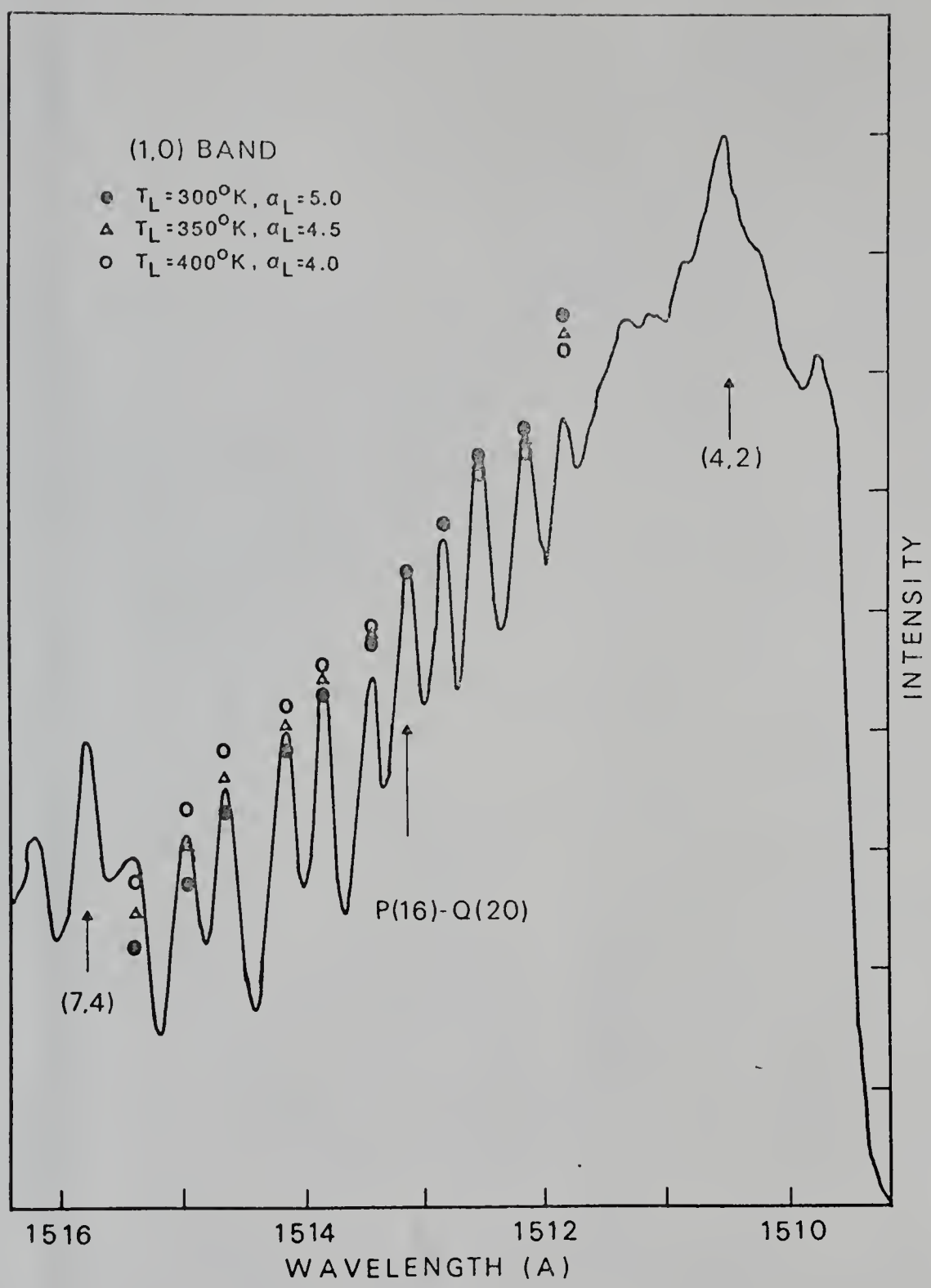
(1,0) BAND
$T_L = 300^oK$, $a_L = 5.0$
$T_L = 350^oK$, $a_L = 4.5$
$T_L = 400^oK$, $a_L = 4.0$
(7,4)
P(16)-Q(20)
(4,2)
INTENSITY
1516
1514
1512
1510
WAVELENGTH (A)

of helium in the monochromator was 5×10^{-5} Torr as indicated by a cold cathode vacuum gauge. CO_2 was then admitted into the lamp until the total pressure in the monochromator was 8 or 9×10^{-5} Torr. The power input to the lamp was set at 80 watts, and the SWR into the microwave cavity was minimized. The monochromator slits were adjusted so that the rotational feature of interest was well resolved. It was found that when this procedure was followed reproducible spectra could be obtained.

The basic features of the (1,0) band are apparent in the spectrum in figure VIII. For $J > 12$ rotational features which consist of one line each from the P, Q, and R rotational branches are resolved. The components of the triplets are of the form P(J), Q(J+4), R(J+9). There are also contributions to the spectrum from two overlapping bands of the fourth positive system. The (4,2) band has a maximum at 1510.4 Å, and the (7,4) band has a maximum at 1515.7 Å. However, both of these bands fall outside of the region of interest for rotational lines investigated in this experiment.

The plotted points in figure VIII are local maxima of the simulated spectra generated by the application of equation 29 to the (1,0) band. The spectra were generated for three different combinations of lamp temperature and absorption coefficient. From the analysis the temperature and absorption coefficient for the discharge were found to be 350°K and 4.5, respectively. The other sets of values were taken to give the experimental limits for these quantities. The simulated spectra were normalized to the experimental spectrum at the P(16),

Q(20), R(25) spectral feature. Once the two lamp parameters were determined the intensities of rotational lines in the exciting radiation were found through the application of equation 28.

Spectra of Scattered Light

A spectrum of scattered resonance radiation was recorded before each run of the level-crossing experiment. Figures IX and X are typical of the spectra obtained for the (1,0) band and (2,0) band, respectively. The plotted points are local maxima of the simulated spectra of scattered light calculated from equation 31. Numerical integration of equation 31 was implemented through the use of an IBM 360 digital computer and a program for computation developed by Wells [30] and Isler [13]. In fitting the simulated spectra to the experimental data, the temperature of the scattering gas was assumed to be 350°K and the absorption coefficient, α_s, was varied to obtain the points plotted in figures IX and X. For the (1,0) band the best fit was judged to be for $\alpha_s = 2.0$. For the (2,0) band the best fit was for $\alpha_s = 3.0$. Both experimental spectra were produced with a scattering gas pressure of 50 microns. As the pressure of the scattering gas was varied from run to run it was of course found that different values of α_s produced better fits to the experimental spectra.

The Hanlé effect signal produced from excitation by the incompletely resolved rotational features of the $v' = 1$ and $v' = 2$ vibrational bands consisted of a superposition of line shapes arising from each excited rotational state of the scattering molecules.

Figure IX: Fluorescent Spectrum of the (1,0) Band

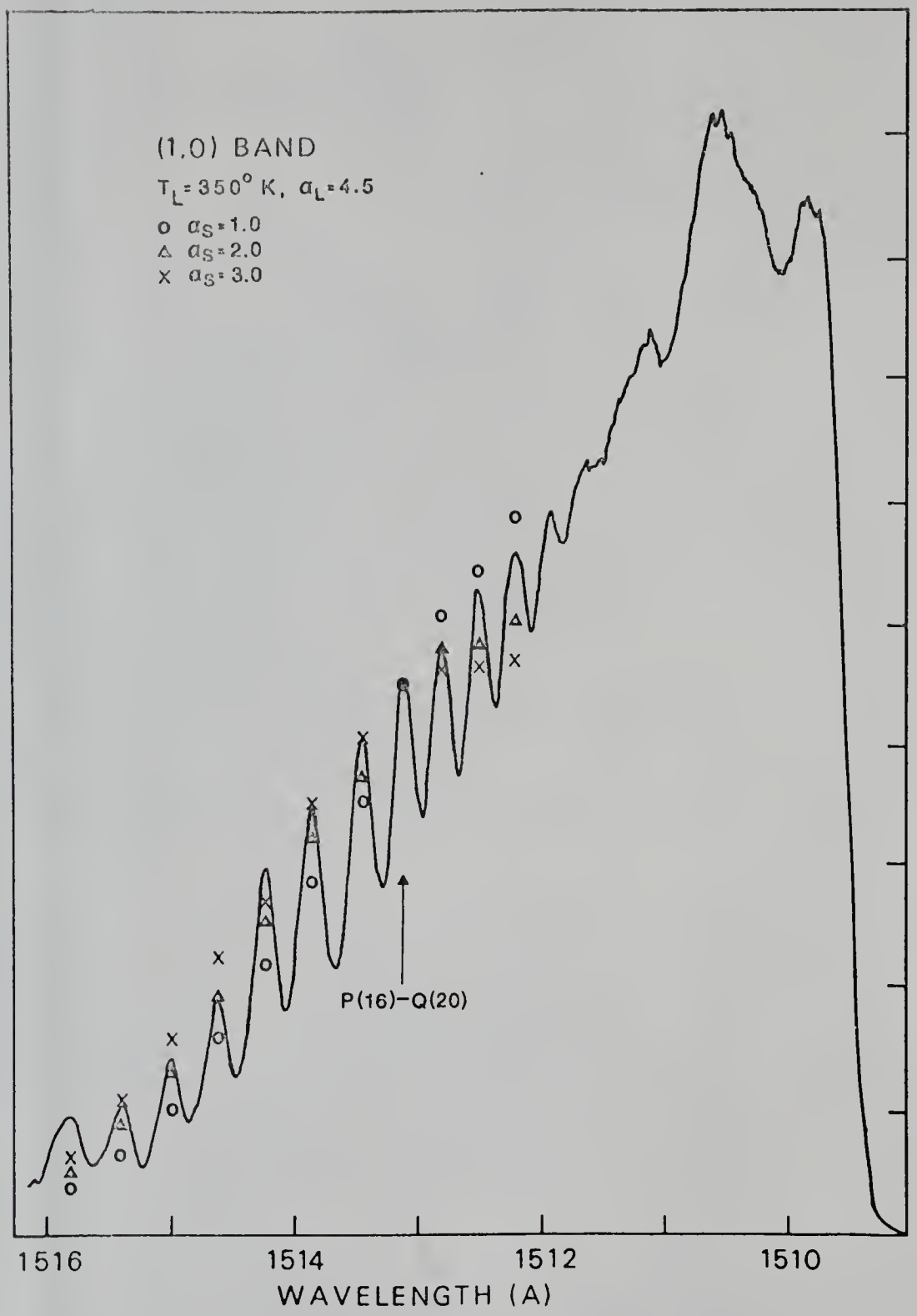
(1,0) BAND
$T_L = 350^\circ$ K, $a_L = 4.5$
o $a_S = 1.0$
Δ $a_S = 2.0$
X $a_S = 3.0$
P(16)–Q(20)
INTENSITY
1516
1514
1512
1510
WAVELENGTH (A)

Figure X: Fluorescent Spectrum of the (2,0) Band

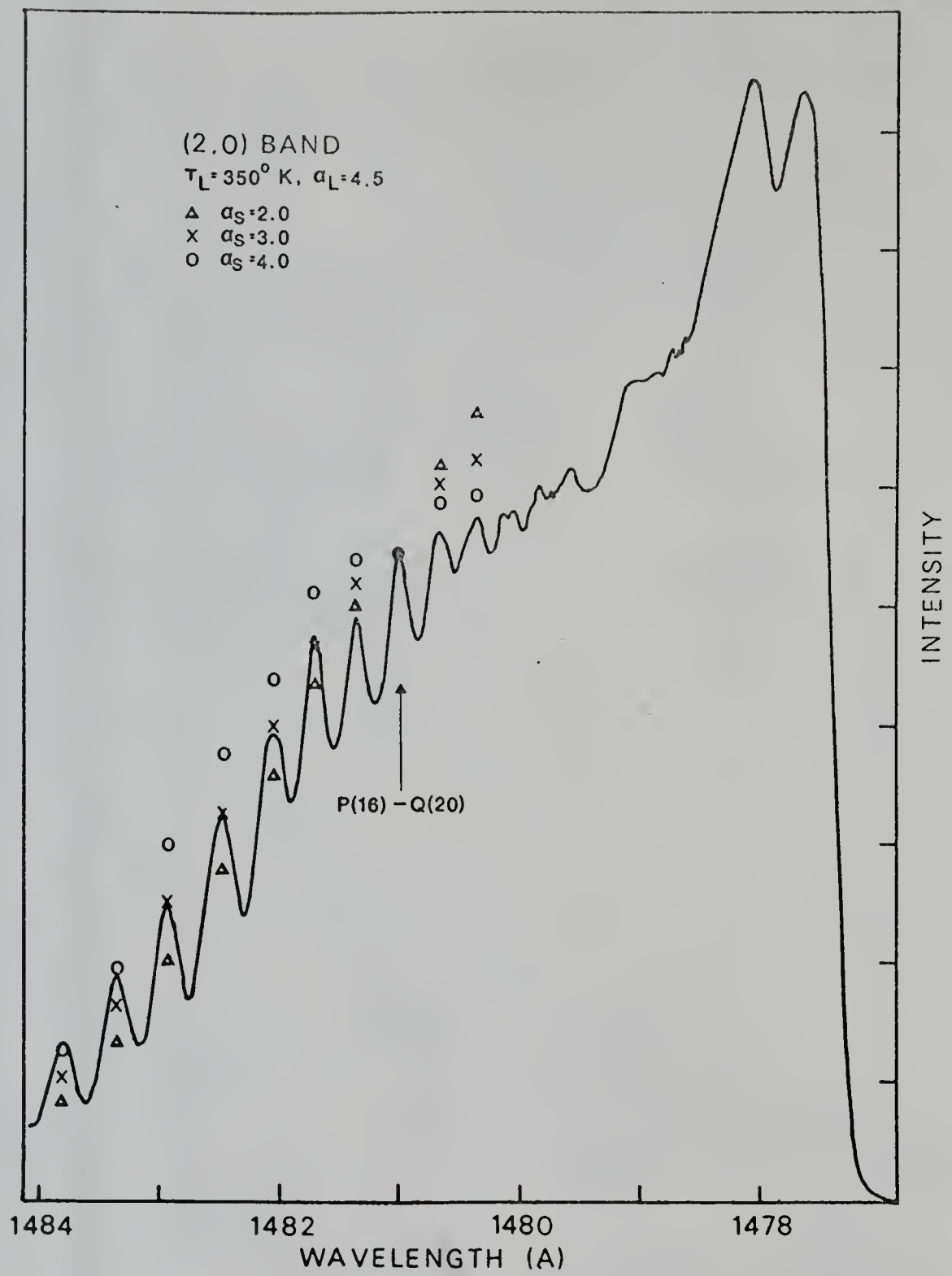
(2,0) BAND
T_L = 350° K, a_L = 4.5
Δ a_S = 2.0
X a_S = 3.0
O a_S = 4.0
P(16) – Q(20)
INTENSITY
1484
1482
1480
1478
WAVELENGTH (A)

The contributions to the Hanlé effect signal were calculated from equation 31 and are listed in Table II. The tabulated figures give the relative contribution to the signal from rotational states excited by a particular branch line. For excitation by a Q branch line, Table I shows that re-radiation from the excited state may be only through a Q branch. For excitation by a P or R branch line, there will be a contribution from re-radiation in both the P and R branches. For the latter case, Table II gives the total contribution from both modes of decay. The contributions to the Hanlé effect signal have been tabulated for three values of α_s for each rotational line of interest. The figures calculated for the bracketing values of the absorption coefficient were taken to give the limits of error in the intermediate value. It may be seen that the contributions to the signal from levels excited by R branch lines are almost negligible.

Analysis of the Hanlé Effect Signals

Analysis of the experimental Hanlé effect lineshapes was carried out on the IBM 360 computer, using a nonlinear least-squares (NLLS) curve fitting program. The theoretical lineshapes to which the signals were fitted consisted of a superposition of a Lorentzian and a dispersion curve for each of the excited rotational states, and a term proportional to the amplitude of the field-independent background. Six parameters were varied simultaneously in the NLLS program to produce the best fit to the experimental data. The rotational levels were assumed to have the same lifetime, and this value was

Table II: Contributions to the Hanlé Effect Signal from Excited Rotational States

Table II

(1,0) Band α_L=4.5 T_L=350° K. Resolution =0.32 A

J	α_S	P(J)	Q(J+4)	R(J+9)
15	1.0	21.2	77.6	1.2
	2.0	19.8	78.3	1.9
	3.0	19.1	78.6	2.4
16	1.0	22.8	76.2	0.9
	2.0	21.2	78.0	0.9
	3.0	20.4	78.4	1.3
17	1.0	25.3	74.2	0.5
	2.0	23.4	75.9	0.7
	3.0	22.0	77.2	0.8
18	1.0	27.7	72.3	0.0
	2.0	25.9	73.7	0.4
	3.0	24.5	75.0	0.5
19	1.0	31.0	69.0	
	2.0	29.6	70.4	0.0
	3.0	28.4	71.6	
20	1.0	34.8	65.2	
	2.0	33.1	66.9	0.0
	3.0	31.9	68.1	
21	1.0	40.0	60.0	
	2.0	38.1	61.9	0.0
	3.0	36.9	63.0	
22	1.0	44.4	55.6	
	2.0	43.6	56.4	0.0
	3.0	42.6	57.4	

Table II continued

(2,0) Band α_L=4.5 T_L=350° K. Resolution =0.32 A

J	α_s	P(J)	Q(J+4)	R(J+9)
15	2.0	19.7	78.3	1.8
	3.0	18.8	78.9	2.2
	4.0	18.1	79.4	2.5
16	2.0	21.2	77.6	1.2
	3.0	20.1	78.4	1.5
	4.0	18.5	79.8	1.7
17	2.0	23.3	76.1	0.6
	3.0	21.8	77.5	0.8
	4.0	20.3	78.8	0.9
18	2.0	25.9	74.6	0.0
	3.0	24.4	75.4	0.2
	4.0	23.0	76.4	0.6

varied to adjust the "halfwidth" of the theoretical curve. In addition, the dispersion curve contributions, the amplitude of the signal, and the ratio of the field-dependent to field-independent terms were adjusted until the experimental and theoretical curves converged. Convergence was judged by monitoring the RMS deviation between the two curves. Deviations of less than 5 percent per point could usually be obtained after eight iterations of the curve fitting program.

Data sets were generally analyzed over intervals of 75 percent and 100 percent of the range of the independent variable, the magnetic field. If the lifetime values predicted by the two fits differed by more than 20 percent, the data were rejected as unreliable. The experimental lifetime values were adjusted to compensate for broadening caused by the time constant present in the detection system. A time constant of 4 percent of the sweep period (a typical value) produced less than 2 percent decrease in the experimental lifetime. The result of an experimental run has been plotted in figure XI along with the fitted curve produced by the NLLS computer program.

Figure XI: Experimental Hanlé Effect Signal with Fitted Lineshape

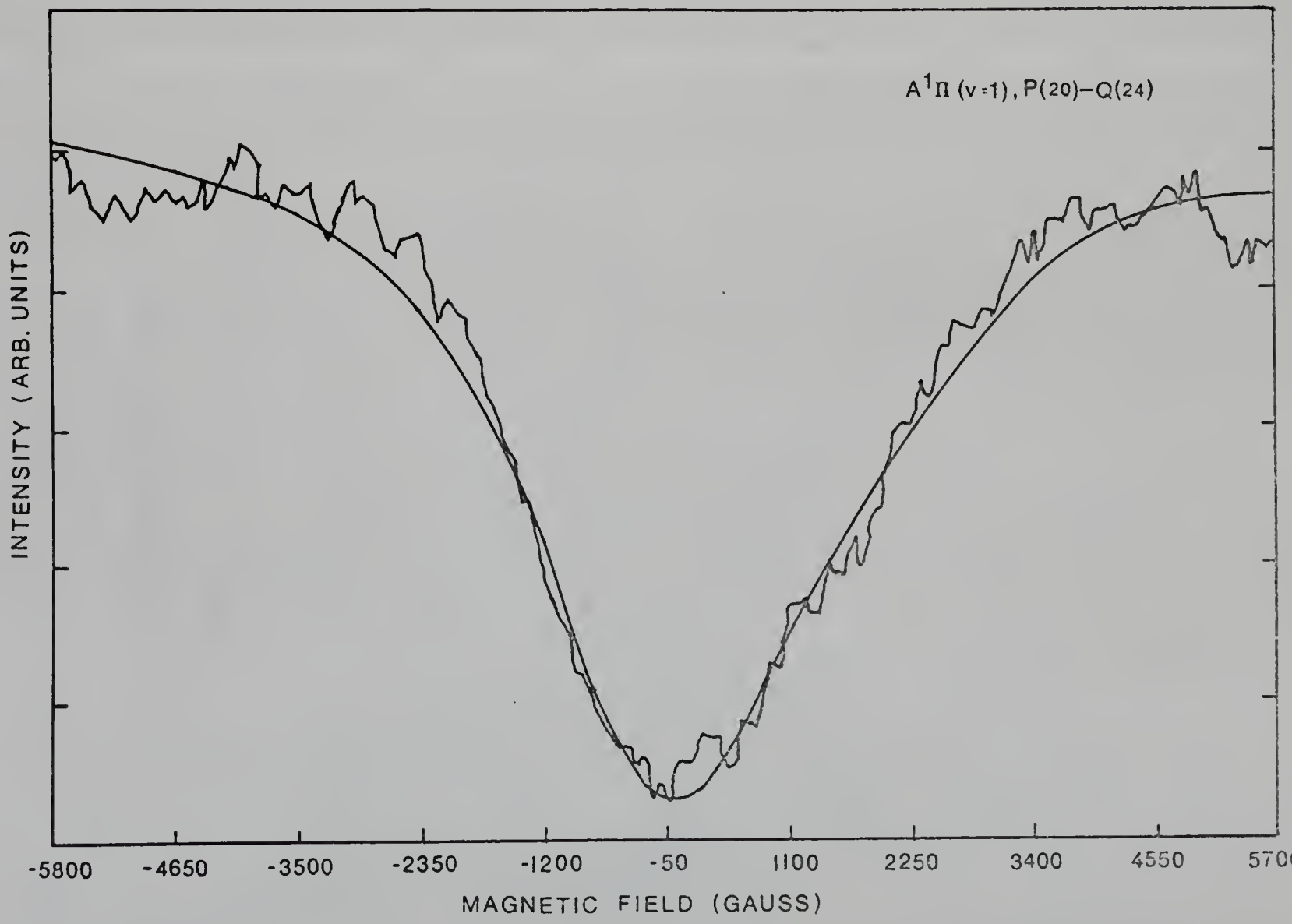
$A^1\Pi$ (v=1), P(20)–Q(24)
INTENSITY (ARB. UNITS)
-5800
-4650
-3500
-2350
-1200
-50
1100
2250
3400
4550
5700
MAGNETIC FIELD (GAUSS)

CHAPTER V

RESULTS

Hanlé effect data were taken on eight resolved rotational features in the (1,0) vibrational band and on four in the (2,0) band. For the (1,0) band, lineshapes from several lines showed pronounced narrowing of their halfwidths due to a perturbation in the $A^1\Pi$ upper state. These data were analyzed separately from those for which the effects of the perturbation were not apparent. For the unperturbed rotational levels the lifetimes derived from the data were averaged to yield the lifetime of the vibrational state. For the (2,0) band, no evidence of narrowing due to perturbations was found for the levels investigated. Measurements of the lifetimes were made for several values of the pressure of the scattering gas for both the $v' = 1$ and $v' = 2$ vibrational levels. No dependence of the measured lifetimes on the scattering gas pressure was detected for either vibrational level for pressures between 50 and 300 microns.

$v' = 1$

Figure XII shows the results of lifetime measurements carried out on the $v' = 1$ vibrational level of the $A^1\Pi$ state. In this figure the product of the lifetime and the Landé g factor, $g_J\tau_J$, is plotted

Figure XII: Experimental Results for the v=1 and v=2 Vibrational Levels

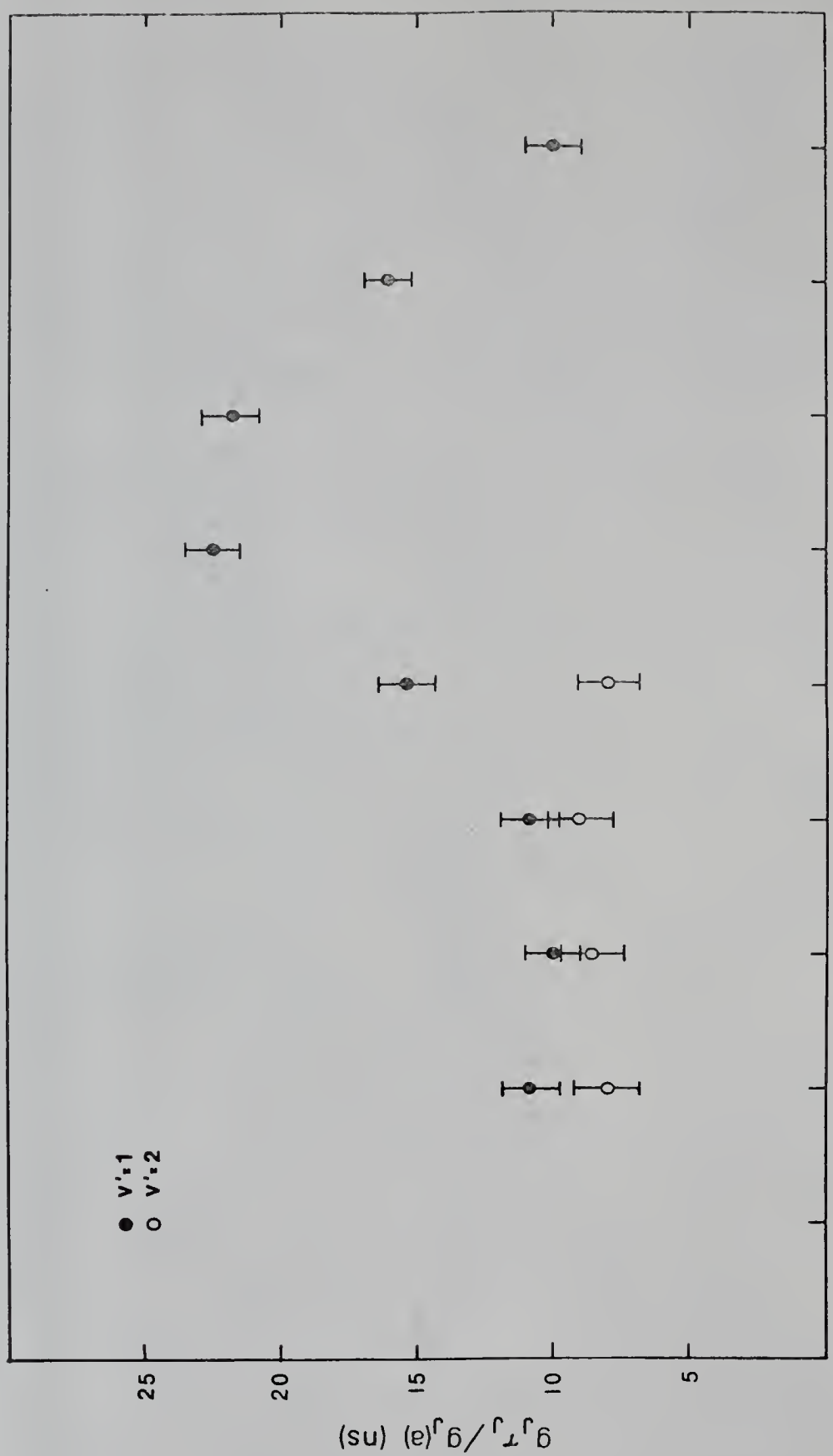
● v'=1
○ v'=2
25
20
15
10
5
$g_J\tau_J/g_J(a)$ (ns)
18
19
20
21
22
23
24
25
26
ROTATIONAL QUANTUM NO. (J)

as a function of the rotational quantum number of the Q branch component of each spectral feature investigated. Since analysis of the Hanle effect lineshapes yielded the product, $g_J\tau_J$, it was necessary to know the Landé g factor in order to ascertain the lifetime of the rotational state. For a $^1\Pi$ molecular state the g factor is found by the application of Hund's case (a) coupling scheme. For case (a) coupling, $g_J = J(J+1)^{-1}$. The data plotted in figure XII have been normalized to these values.

Results for Unperturbed Levels

The measured lifetimes of rotational features characterized by Q branch lines for which $J' = 19$, 20, 21, and 26 were averaged to yield the lifetime of the $v' = 1$ vibrational state. The result was

$$\tau_{v'=1} = 10.41 \pm 0.8 \text{ nanoseconds.}$$

The lifetimes plotted in figure XII represent averages of two or three runs, each between two and four hours long. The error bars plotted represent the deviation from the mean of the averaged values. In all cases deviations of about 10 percent were obtained. The error quoted for the experimental lifetime is the square root of the sum of the squares of the estimated random errors incurred in the experiment. Contributions to this figure were from the three following sources: (1) Uncertainty in the range of the magnetic field sweep. This error was estimated to be, at most, 4 percent of the total range of the field. (2) Variation among measured lifetimes derived from

individual runs. For the $v' = 1$ measurement this error was taken to be the mean deviation from the mean of the measured lifetimes and amounted to 5 percent of the average value. (3) Uncertainty inherent in the analysis of the contributions to the level-crossing signal from unresolved rotational levels. This error may be estimated from Table II. The maximum deviation from the estimated value for any of the contributions tabulated is less than 5 percent. Further, it may be shown that a 5 percent deviation in the contribution to the level-crossing signal from one of the unresolved rotational levels will cause only a 2 percent deviation in the experimental lifetime. The experimental error, ϵ, may therefore be written as

$$\epsilon = [(4)^2 + (5)^2 + (2)^2]^{\frac{1}{2}} \% = 6.7\% .$$

Results for Perturbed Levels

The pronounced increase in the product, $g_J \tau_J$, for levels adjacent to $J = 23$ is believed to result from a perturbation which couples the $A\,^1\Pi, v' = 1$ state to another state of the molecule. Simmons et al. [2] have attributed a perturbation which has a maximum in the Q branch at $J = 23$ to the $a'\,^3\Sigma^+ F_1(v' = 10)$ state. The notation, F_1, designates the component of the triplet for which $J = N + 1$, where N is the quantum number for the total angular momentum apart from spin. This state perturbes the $^1\Pi$ state by a spin-orbit interaction for which the selection rule, $\Delta J = 0$, holds [27,39]. The theory outlined above for the analysis of level-crossing signals from perturbed states was applied to lineshapes from those rotational

features containing Q branch lines for which $J' = 22$, 23, 24, and 25. In fitting lineshapes from perturbed rotational features only the product, $g_J\tau_J$, for the perturbed Q branch upper state was varied to obtain the fit. The lifetime of the other two components was taken to be that of the $v' = 1$ state (10.41 nanoseconds). The Landé g factor for the $^3\Sigma^+$ perturbing state is given by Hund's case (b) coupling scheme. For the F_1 component of the $^3\Sigma^+$ state, $g_J = 2/J$. The results of the analysis of the perturbed levels are given in Table III. The coupling coefficients, α and β, were first calculated from equation 52 using the experimental value of $H_{\frac{1}{2}}$. Employing the value of α, the lifetime and effective g factor for the perturbed level were calculated from equations 50 and 48, respectively. The values of Δ, the matrix element of the perturbation between the $^1\Pi$ and $^3\Sigma^+$ states, were obtained by application of equation 43.

$v' = 2$

The measured lifetimes of rotational features containing Q branch lines for which $J' = 19$, 20, 21, and 22 were averaged to yield the lifetime of the $v' = 2$ vibrational state. The result was

$$\tau_{v'=2} = 8.49 \pm 1.0 \text{ nanoseconds.}$$

Results of the lifetime measurements on the $v' = 2$ state have been plotted in figure XII. The error bars give the uncertainty in the results for the individual rotational levels. The uncertainty amounts to about 12 percent of the experimental values. No functional dependence of the lifetime on the rotational quantum number is apparent

Table III: Experimental Results for Perturbed Rotational Levels

Table III

J	α	β	$\Delta(cm^{-1})$	τ_J(ns)	g_J/g_J(a)
22	.994	.108	3.36	10.52	1.47
23	.987	.159	1.55	10.69	2.13
24	.988	.152	2.17	10.67	2.05
25	.994	.108	3.80	10.52	1.53

for the levels investigated. Simmons et al. [2], in fact, report no perturbations in either the Q or P branches for values of J between 10 and 25. The uncertainty in the experimental lifetime is due almost entirely to statistical fluctuation in the measured results from the individual rotational levels.

CHAPTER VI

CONCLUSIONS

Level-crossing spectroscopy has been shown to be a useful technique for the investigation of certain fundamental properties of excited molecular states. The measured lifetimes obtained in this experiment were found to be in very good agreement with those obtained by other investigators as may be seen from Table IV. The agreement with the results of Wells and Isler [13] is particularly interesting. The Hanlé effect signals produced in their investigation resulted from transitions from the first eight rotational levels of the $v' = 2$ vibrational state. In both experiments, however, the technique of analysis of the observed lineshapes was similar and the agreement between the lifetime values obtained for small and large rotational quantum numbers affords credibility to the technique.

Hesser's [11] lifetime values were obtained by the direct observation of the decay of upper states of the four positive system excited by electron impact of carbon monoxide. The results seem consistently large, however, and may contain systematic error introduced by undetected cascading transitions from higher excited states. Imhof and Read [18] have eliminated the problem of cascading through the use of the delayed coincidence technique. In monitoring the decay of the excited states, no photon was counted which was not

Table IV: Lifetimes of Vibrational Levels of the A State of CO

Table IV

v'	This work	Wells and Isler[a]	Hesser[b]	Imhof and Read[c]	Chervenak and Anderson[d]
1	10.41 ± 0.8 ns.	----------	10.90 ± 0.2 ns.	10.37 ± 0.3 ns.	16.2 ns.
2	8.49 ± 1.0 ns.	9.0 ± 1.0 ns.	10.5 ± 1.0 ns.	9.35 ± 0.25 ns.	16.6 ns.

a. Reference 13

b. Reference 11

c. Reference 18

d. Reference 19

correlated to a particular scattered electron responsible for the excitation of the state.

The lifetime results of Chervenak and Anderson [19] were obtained by using a pulsed invertron [40] excitation source and a delayed coincidence measurement technique [41]. The large discrepancy between their results and those of the other investigators may be attributable to one or more of the following explanations: (1) Cascading. The $B^1\Sigma^+$ state of carbon monoxide lies above the $A^1\Pi$ state and has a lifetime of about 24 nanoseconds. Cascading transitions from the $B^1\Sigma^+$ state would be difficult to detect and could cause an increase in the apparent lifetime of the $A^1\Pi$ state. (2) Radiation trapping. The invertron was operated with carbon monoxide pressures of from 50 to 500 microns and at a temperature of about 900°K. Under these conditions it is probable that resonance trapping of the escaping radiation occurred. The trapping process could produce a marked increase in the apparent lifetimes of states participating in resonance transitions. (3) Slow system response. The pulsed invertron technique has not been applied to the measurement of lifetimes in the 10 nanosecond range. It is possible that the system is limited to a response time of around 15 nanoseconds and therefore could not "follow" the decay of the $A^1\Pi$ state

The variation of the radiative lifetime with the vibrational level found in this work and that of Imhof and Read is significant. These results indicate a dependence of the electronic transition moment on the internuclear separation in the carbon monoxide molecule.

Unfortunately, the observed decrease in the lifetime from $v' = 1$ to $v' = 2$ is not consistent with the dependence of the transition moment on the r-centroid bound by Mumma et al. [14] given in equation 1. This relation produces a slight increase in the lifetime with the vibrational level. Theoretically, the trend in the lifetimes is very sensitive to the slope of the transition moment versus the r-centroid curve so that a slight adjustment of equation 1 might produce agreement with the lifetime results. It is also possible that the transition moment has a higher than linear dependence on the r-centroid, although this dependence cannot be inferred from the results of the present experiment.

The sensitivity of the level-crossing technique is demonstrated by the results for the perturbed levels of the $v' = 1$ vibrational level. The experimental values of the coefficients, α and β, show the coupling between the $^1\Pi$ and $^3\Sigma^+$ states to be rather small even at the maximum of the perturbation. Additional lines in the spectrum of the (1,0) band were reported by Simmons et al. [2] only for $J' = 23$ and $J' = 24$, but the effect of the perturbation was clearly evident in the level-crossing data for four different rotational levels. The sensitivity of the Hanlé effect lineshapes to the perturbation may be accounted for by the fact that the halfwidth of the signal is proportional to $(g_J \tau_J)^{-1}$. While the perturbation left the lifetimes of the affected levels unchanged, the effective g values were found to increase by as much as a factor of two over the values predicted for the $^1\Pi$ state by case (a) coupling. The values of Δ listed in Table III show a dependence on the rotational quantum numbers of the perturbed levels,

but this variation is almost certainly introduced by statistical uncertainty in the data. The mean for these values was

$$\Delta = 2.7 \text{ cm}^{-1}$$

and is in agreement with values which may be obtained from conventional spectroscopic analysis.

LIST OF REFERENCES

1. P. H. Krupenie, The Band Spectrum of Carbon Monoxide, National Standard Reference Data Series (1966).

2. J. D. Simmons, A. M. Bass, and S. G. Tilford, Astrophys. J. 155, 345 (1969).

3. G. Herzberg and T. J. Hugo, Canadian J. Phys. 33, 125 (1955).

4. J. D. Simmons and S. G. Tilford, J. Chem. Phys. 45, 2965 (1966).

5. G. Herzberg, J. D. Simmons, A. M. Bass, and S. G. Tilford, Canadian J. Phys. 44, 3039 (1966).

6. L. Goldberg, W. H. Parkinson, and E. M. Reeves, Astrophys. J. 141, 1293 (1965).

7. T. P. Stecher and P. A. Williams, Astrophys. J. 146, 88 (1965).

8. C. Barth, Science 165, 1004 (1969).

9. C. Barth, J. Geophys. Res. 76, 2213 (1971).

10. T. C. James, "Transition Moments, Franck-Condon Factors, and Lifetimes of Forbidden Transitions. Calculation of the Intensity of the Cameron System of CO.," to be published.

11. J. E. Hesser, J. Chem. Phys. 48, 2518 (1968).

12. V. Meyer, A. Skerbele, and E. Lassettre, J. Chem. Phys. 43, 805 (1965).

13. W. C. Wells and R. C. Isler, Phys. Rev. Letters 24, 705 (1970).

14. M. J. Mumma, E. J. Stone, and E. C. Zipf, J. Chem. Phys. 54, 2627 (1971).

15. G. M. Lawrence, Bull. of the Am. Phys. Soc. 16, 204 (1971).

16. E. Lassettre and A. Skerbele, J. Chem. Phys. 54, 1597 (1971).

17. V. Meyer and E. Lassettre, J. Chem. Phys. 54, 1608 (1971).

18. R. E. Imhof and F. H. Read, Chem. Phys. Letters 11, 326 (1971).

19. J. G. Chervenak and R. A. Anderson, J. Opt. Soc. Am. 61, 952 (1971).

20. W. Hanlé, Z. Physik 30 (1924).

21. G. Breit, Rev. Mod. Phys. 5, 91 (1933).

22. F. D. Colgrove, P. A. Franken, R. R. Lewis, and R. N. Sands, Phys. Rev. Letters 3, 420 (1959).

23. R. Zare, J. Chem. Phys. 45, 4510 (1966).

24. P. R. Crosley and R. Zare, Phys. Rev. Letters 18, 942 (1967).

25. R. deZafra, A. Marshall, and H. Metcalf, Phys. Rev. A 3, 1557 (1971).

26. S. G. Silvers, T. H. Bergeman, and W. Klemperer, "The Optical Detection of Zero Field Level Crossing in the $A^1\Pi$ State of CS" (Twenty-Third Symposium on Molecular Structure and Spectroscopy, Columbus, Ohio, Sept. 3-7, 1968).

27. A. R. Edmonds, Angular Momentum in Quantum Mechanics (Princeton, N. J., 1960).

28. H. Conroy, "Molecular Schrodinger Equation VIII. A New Method for the Evaluation of Multidimensional Integrals" (Mellon Institute, Theoretical Chemistry Preprint No. 24, July 10, 1967).

29. G. Herzberg, Molecular Spectra and Molecular Structure I. Spectra of Diatomic Molecules (D. Van Nostrand Co., Inc., Princeton, N. J., 1950), 2nd ed.

30. W. C. Wells, "Level-Crossing Spectroscopy of Diatomic Molecules: Application to an Excited State of Carbon Monoxide," Ph.D. dissertation, University of Florida (1969).

31. D. K. Anderson, Phys. Rev. A 137, 21 (1965).

32. H. Okabe, J. Opt. Soc. Am. 54, 478 (1964).

33. R. G. Taylor, T. A. Chubb, and R. W. Kriplin, J. Opt. Soc. Am. 55, 107S (1965).

34. D. F. Heath and P. A. Sacher, Appl. Optics 5, 937 (1966).

35. P. Warneck, J. Opt. Soc. Am. 55, 921 (1965).

36. R. A. Young, G. Black, and T. G. Slanger, J. Chem. Phys. 48, 2067 (1968).

37. J. D. Jackson, Classical Electrodynamics (John Wiley and Sons, Inc., New York, 1962), p. 254.

38. F. C. Fehsenfeld, K. M. Evenson, H. P. Broida, Rev. Sci. Instr. 36, 294 (1965).

39. I. Kovacs, Canadian J. Phys. 36 (1958).

40. T. M. Holzberlein, Rev. Sci. Instr. 35, 1041 (1964).

41. J. Z. Klose, Phys. Rev. 141, 181 (1966).

BIOGRAPHICAL SKETCH

Ralph Laurence Burnham was born April 16, 1944, in Jacksonville, Florida. In June, 1962, he was graduated from Terry Parker High School. In June, 1966, he received the degree of Bachelor of Science with a major in Physics from the Georgia Institute of Technology. In 1966 he enrolled in the Graduate School of the University of Florida. He worked as a graduate assistant in the Department of Physics until March, 1972. From September, 1966, until the present time, he has pursued his work toward the degree of Doctor of Philosophy.

Ralph Laurence Burnham is a member of the Tau Beta Pi Society.

I certify that I have read this study and that in my opinion it conforms to acceptable standards of scholarly presentation and is fully adequate, in scope and quality, as a dissertation for the degree of Doctor of Philosophy.

Ralph C. Isler, Chairman
Associate Professor of Physics

I certify that I have read this study and that in my opinion it conforms to acceptable standards of scholarly presentation and is fully adequate, in scope and quality, as a dissertation for the degree of Doctor of Philosophy.

Charles F. Hooper, Jr.
Associate Professor of Physics

I certify that I have read this study and that in my opinion it conforms to acceptable standards of scholarly presentation and is fully adequate, in scope and quality, as a dissertation for the degree of Doctor of Philosophy.

Thomas A. Scott
Professor of Physics

I certify that I have read this study and that in my opinion it conforms to acceptable standards of scholarly presentation and is fully adequate, in scope and quality, as a dissertation for the degree of Doctor of Philosophy.

Thomas L. Bailey
Professor of Physics

I certify that I have read this study and that in my opinion it conforms to acceptable standards of scholarly presentation and is fully adequate, in scope and quality, as a dissertation for the degree of Doctor of Philosophy.

William W. Weltner, Jr.
Professor of Chemistry

This dissertation was submitted to the Department of Physics & Astronomy in the College of Arts and Sciences and to the Graduate Council, and was accepted as partial fulfillment of the requirements for the degree of Doctor of Philosophy.

March, 1972

Dean, Graduate School

JM7 1.6 25.8.